9.1 What Are Network Solids?

9.1.1 Concepts and Classification

Moulton, B. and Zaworotko, M. J., 'From molecules to crystal engineering: Supramolecular isomerism and polymorphism in network solids', *Chem. Rev.* 2001, **101**, 1629–1658.

So far we have been predominantly focused on the host-guest paradigm of supramolecular chemistry. In Chapters 3–6 we looked at discrete, solution phase hosts for various guests. In Chapter 7 we focused on (predominantly organic) molecular crystalline solids with guest binding cavities or channels and in the last chapter we developed this solid state chemistry into crystal engineering – designer solids based on supramolecular interactions. Now that we have seen that it is possible to understand and engineer molecular solids we turn to infinite solid-state networks where, formally, there are no discrete molecules and the entire solid is either all one molecule (as in diamond) or made up of relatively few infinite polymeric strands linked together by strong covalent, or more commonly, dative coordination bonds. Into this category fall naturally occurring inorganic materials such as zeolites as well as a vast range of coordination polymers – infinite coordination complexes in which metal ions are bridged by multidentate ligands into an infinite line or array. Some of these materials (*e.g.* zeolites) have cavities and are porous and so act as hosts for guests in the way we saw organic hosts do in Chapter 7. Others are not hosts but are still interesting from the point of view of materials design using supramolecular interactions or templating. In this chapter we progress from frameworks for capture, storage or transport that are often only stable in the presence of guests (*i.e.* clathration – the process of transforming a dense crystal form to an open structure containing the guest) to materials that take up guests reversibly without a major alteration in host structure (*i.e.* sorption – relatively facile diffusion of guests into a structure with permanent void space). At the interface between these extremes is nascent interest in host materials that respond to an external stimulus in a controlled fashion. This kind of dynamic 'smart' sorbent exhibits more complicated behaviour with significant changes at both the crystal and molecular levels.

In this chapter we begin with some relatively classical materials that are well-known and move on to the latest research in coordination polymers, particularly *metal-organic frameworks* that exhibit remarkable structural robustness in comparison to traditional clathrates, yet are highly amenable to design and modification, in contrast to the inorganic zeolites. In reaching this point we have come on a long journey following the science of non-covalent interactions, from solution host-guest chemistry, which has been traditionally the preserve of synthetic organic chemists or coordination chemists, through the physical organic chemistry of clathrates all the way to what is really a branch of modern materials science. This breadth of supramolecular chemistry is at once one of its most daunting yet exciting features.

For convenience we will classify network solids according to the dimensionality of their connectivity as listed below, where connectivity in this context refers to a strong covalent or coordination bond. Some examples are shown in Figure 9.1.

- 0D solids comprise discrete molecules – these are the kinds of compound we considered in the last chapter.
- 1D solids comprise infinite thread-like strands. The solid is then made up of the non-covalent packing of these strands.
- 2D solids are made up of sheet-like components that are infinite in two dimensions and pack together *via* non-covalent interactions in the third.

Supramolecular Chemistry, 2nd edition J. W. Steed and J. L. Atwood
 ISBN: 978-0-470-51233-3

- 3D solids are fully three-dimensionally interconnected covalent or coordination compounds in which the entire crystal is formally a single molecule.

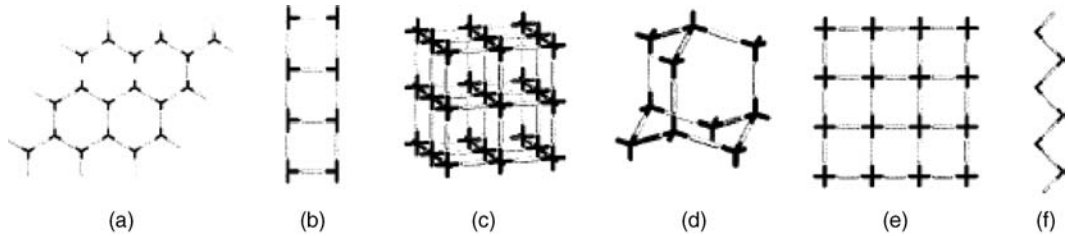

Figure 9.1 Schematic representation of some of the simple network architectures structurally characterised for metal-organic polymers: (a) 2D honeycomb, (b) 1D ladder, (c) 3D octahedral, (d) 3D hexagonal diamondoid, (e) 2D square grid, and (f) 1D zigzag chain (reprinted from Section Key Reference © The American Chemical Society).

Within these categories we will also distinguish between materials that are either *porous* or *non-porous* according to strict definitions that we will discuss in Section 9.1.3, and whether or not individual networks are *interpenetrated* (in one, two or three dimensions) with other networks – *i.e.* whether they are mutually topologically entangled in such a way that they could not be separated without breaking bonds. We begin with a description of nomenclature that we will use to describe network topology.

9.1.2 Network Topology

Robson, R., 'A net-based approach to coordination polymers', *J. Chem. Soc., Dalton Trans.* 2000, 3735–3744.

Topology is a basic field of mathematics in which any network is reduced to a series of nodes (connection points) and connections. Networks are said to be topologically equivalent unless they cannot be deformed into one another without cutting or glueing. Thus the topology of networks depends on the way in which they are connected, not on the shape or size of the individual components. The science of topology began with Leonhard Euler's solution to the *seven bridges of Königsberg* problem. Königsberg (now Kaliningrad in Russia) was the capital of East Prussia and is built on the River Pregel at the junction with another river. The island of Kniephof is situated at the conflux of the two rivers. The island and different parts of the mainland are mutually linked by a total of seven bridges, Figure 9.2. The problem

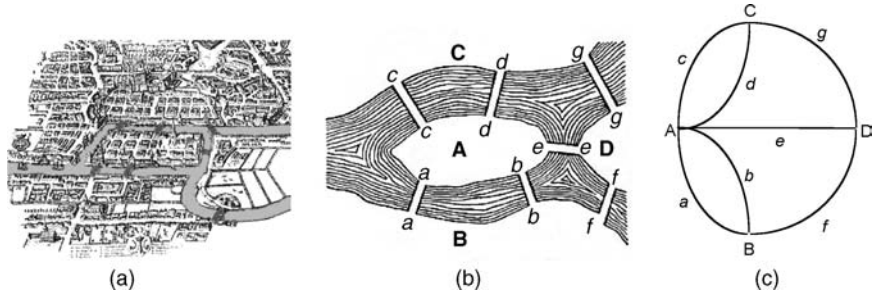

Figure 9.2 (a) The City of Königsberg showing the seven bridges. The island of Kniephof is in the centre. (b) simplified map and, (c) topological representation where land masses are reduced to nodes and bridges are reduced to lines.

is to cross all seven bridges without crossing any one twice. In 1735, Euler presented the solution to the problem to the Russian Academy, proving that crossing all seven bridges without crossing a bridge twice is impossible. Euler's solution was based on his invention of graph theory, from which, in turn topology developed. He reasoned that every land mass muct have an even number of bridges allowing a traveller to get on and off again. In fact each land mass has an odd number.

As far as real network solids go, we can reduce chemical entities such as metal centres or small clusters of metals (termed *secondary building units* or SBUs) to nodes, and bridging ligands to connections. It then becomes possible to describe the topology of a chemical network material. In a famous book published in 1977 A. F. Wells identified a number of commonly occurring chemical network topologies[1] and many more are now known, although presumably more remain to be discovered. Network topologies may be described by two somewhat related sets of symbols or notation, and it is easy to become confused between them.

Wells notation takes the form (n, p)-net where n and p are integers that describe, respectively, the shortest route in terms of number of nodes to complete a circuit back to the starting place and the connectivity of a given node. Thus a (6,3)-net contains hexagonal holes (or, if irregular, holes that form a six-sided polygon; a 6-gon; $n = 6$) and each node is 3-connected ($p = 3$).

A *Schläfli symbol* describes the length of the shortest routes, in terms of number of nodes, from one node back to itself based on each pair of connections at the node. For example, the Schläfli symbol 6^3 means that 6-gons are the shortest circuit of connecting nodes that can be formed, and that there are three of these circuits radiating out in different directions from each node. Similarly the symbol 4.8^2 indicates that the shortest circuit back to a three-connected node is a 4-gon between one pair of connections and two 8-gons between the other two pairs. Some common network topologies and their Schläfli symbols are given below. Note how the hexagonal grid and 'brick wall' patterns are topologically identical – they are both 6^3 (or (6,3) in Wells' system) networks. The two sets of symbols are not always the same, however. For a square grid based on a square planar metal centre node for example, the Wells nomenclature is (4,4). In the Schläfli nomenclature this network would be described as $4^4.6^2$ – there are four pairs of *cis* related connections giving four 4-gons (squares in the example shown in Figure 9.3 but there are also two pairs of *trans* related connections giving

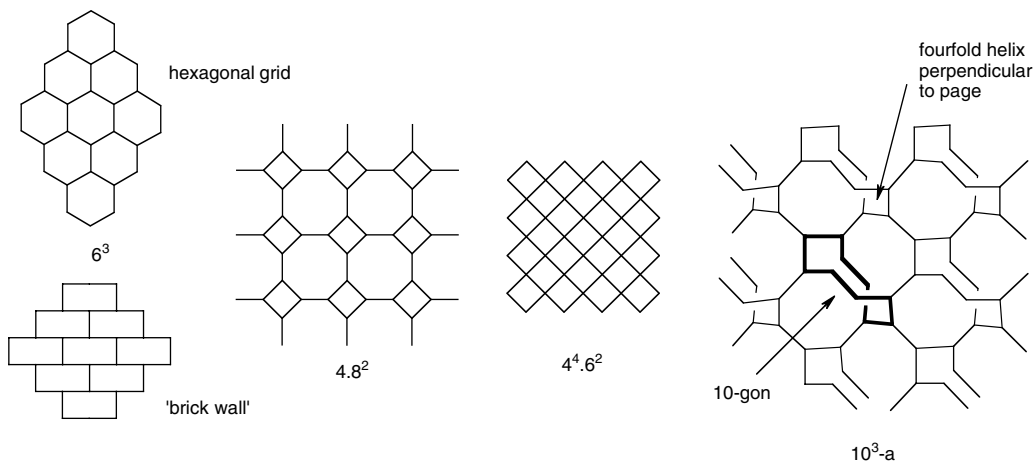

Figure 9.3 Examples of network topologies along with their Schläfli symbols. The corresponding Wells symbols are (6,3), ($4,8^2$), (4,4) and (10,3)-a.

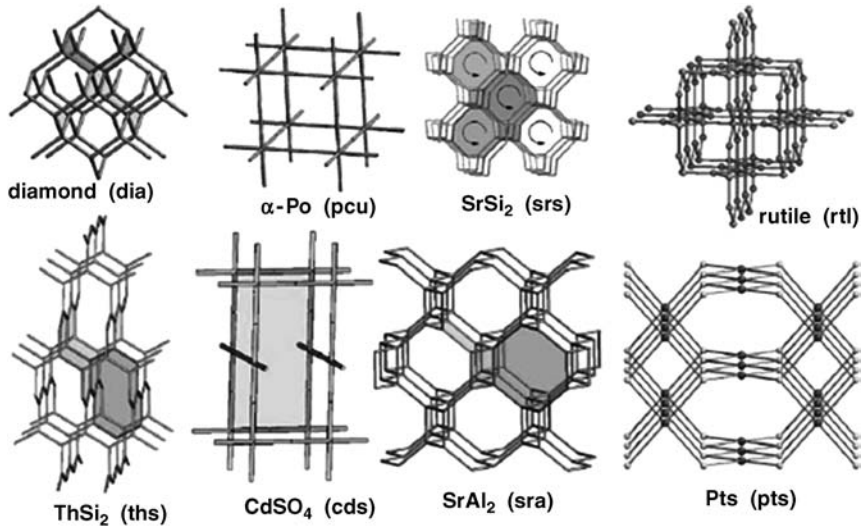

Figure 9.4 Common nets exhibited by simple materials along with their generic names. Characteristic rings are shaded. The $SrSi_2$ structure is a (10,3)-a net (reproduced with permission from The Royal Society of Chemistry). See plate section for colour version of this image.

two 6-gons (rectangles). The Wells and Schläfli nomenclature can become complicated in three dimensions and for complex topologies, particularly when more than one topologically distinct type of node is present (the nets shown in Figure 9.3 are all examples of uninodal nets; nets with two, three or more types of node are termed binodal, trinodal *etc*.). For nets that are common, recognised types a trivial name based on the simplest representative member of the series is often adopted (Figure 9.4). For example diamondoid (4-connected tetrahedral centres, Section 8.12), α-polonium (or NaCl, with 6-connecting, octahedral centres), the NbO net (square planar 4-connecting centres with a 90° rotation along each connection); the PtS net (with a 1 : 1 ratio of tetrahedral and square planar nodes), the rutile net (octahedral and trigonal centres in a 1 : 2 ratio); the 'Pt_3O_4' net (with square planar and trigonal nodes in a 3 : 4 ratio) and the Ge_3N_4 net (with tetrahedral and trigonal nodes in a 3 : 4 ratio).

Another interesting net is the cubic (10,3)-a (Wells) or 10^3-a (Schläfli) net exhibited by $SrSi_2$. This may be regarded as a three-connected analogue of the four-connected, cubic diamondoid net. The 'a' refers to the most symmetrical variant of (10,3) nets identified by Wells. The (10,3)-a net is chiral with fourfold screw axes (Box 8.2) running through the structure. An nice example is the zinc(II) tripyridyltriazine (**9.1**) complex $[Zn(\mathbf{9.1})_{2/3}(SiF_6)(H_2O)_2(MeOH)] \cdot$ solvent. In this case the Zn(II) ions are each bound to two tripyridyltriazine ligands and so act as essentially linear connectors (the zinc coordination environment is completed by bonds to two water molecules, the SiF_6^{2-} anion and a methanol molecule, none of which matter from a topological point of view). As a result it is the tripyridyltriazine ligands that we think of as being the 3-connected nodes. The network structure actually comprises eight interpenetrating (10,3)-a nets, four of each handedness. The environment about one of the fourfold helices is shown in Figure 9.5.

Recently there have been significant advances in mathematical tiling theory which have been applied to more rigorous descriptions of complex 3D (or 3-*periodic*) network topologies. The reader is referred to the literature for a complete description of these powerful new methods.[3, 4]

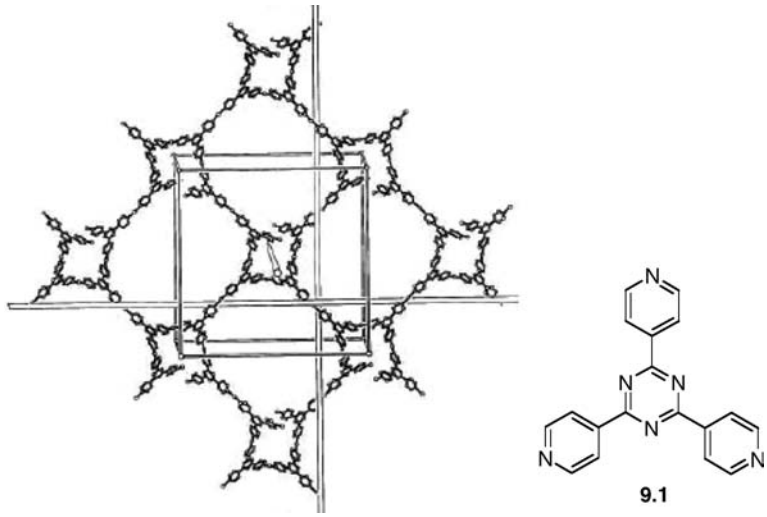

Figure 9.5 The view along the fourfold helix in one of the eight interpenetrating (10,3)-a nets in $[Zn(\mathbf{9.1})_{2/3}(SiF_6)(H_2O)_2(MeOH)]\cdot$solvent. Helices are highlighted by imaginary poles running along the selected helical axes (reproduced with permission from The Royal Society of Chemistry).

9.1.3 Porosity

Barbour, L. J., 'Crystal porosity and the burden of proof', *Chem. Commun.* 2006, 1163–1168.

The presence or absence of 'porosity' in solids is of crucial interest in their ability to function as host materials for any substance, be it liquid, solid or gas under ambient conditions. Porous materials have very broad applications in catalysis, separations and sequestration applications and are an area of tremendous current interest. Len Barbour of the University of Stellenbosch, South Africa, identifies two key criteria (listed below) that must be fulfilled if a material is to be described as porous.

1. Permeability should be demonstrated (*e.g.* by gas sorption measurements, spectroscopic evidence of guest exchange or crystallography).
2. The term 'porous' should apply to a specific host phase and not simply to the host molecules as an amorphous or mutating collective. Therefore, in principle, the host framework should remain *substantially unaffected* by guest uptake and removal. This requirement means that we do not describe, for example, the close-packed, tetragonal α-phase of urea as porous, however the description would be appropriate for an empty, hexagonal urea β_0 apohost phase (Section 7.3)

Given these requirements Barbour identifies three kinds of porosity in the current literature:

1. porosity 'without pores',
2. conventional porosity,
3. virtual porosity.

We have already seen in Section 7.9 a number of systems exhibiting porosity 'without pores'. This term applies to generally relatively soft solids such as molecular clathrates that can deform in such a way as to allow the ingress and egress of guest molecules without any obvious channel or port in the

conventional space-filling representation of the structure of the material. Porosity without pores is a real and useful phenomenon and the reader is referred to Section 7.9 for a description of some of the fascinating compounds exhibiting this kind of behaviour. In this chapter we will focus much more on conventional porosity. Conventional porosity requires the existence of permanent, linked gaps or holes in a solid with a minimum diameter of about 3 Å, and a size typically in the region 3–10 Å for microporous solids. In Section 7.9 we identified the various categories of micro- meso- and macroporous solids and the size ranges of the pores they possess. Note however that pore size, particularly in microporous solids, is somewhat dependent on how it is measured. The usual method involves choosing a 'probe' of arbitrary radius (*e.g.* 1.1 Å the radius of a hydrogen atom) and computationally rolling the probe around the van der Waals surface of the void space and measuring the volume swept out using software such as MSROLL. The result is clearly dependent on the choice of probe radius! Conventional porosity is exhibited by compounds such as zeolites and is of tremendous academic and industrial interest. The third category, virtual porosity, is not a category of porosity at all according to the definitions given above, but rather a warning to researchers to beware misleading pitfalls. Virtual porosity can come about by the appearance of a pore or cavity if a crystal structure is viewed in ball-and-stick mode but disappears if viewed in van der Waals space-filling mode. Virtual pores can also be created by artificially not showing a component that the naïve user designates as a 'guest' even if that guest is necessary for the maintenance of the structure, *e.g.* counter anions. Thankfully publications exhibiting this false, 'virtual' kind of porosity are rare!

9.2 Zeolites

Web site of the International Zeolite Association: http://www.iza-online.org/. This resource contains a comprehensive database of manipulable 3D zeolite structures.

9.2.1 Composition and Structure

Čejka, J., 'Zeolites: structures and inclusion properties', in *Encyclopedia of Supramolecular Chemistry*, Atwood, J. L., Steed, J. W., eds. Marcel Dekker: New York, 2004; Vol. 2, *pp.* 1623–1630.

Zeolites are naturally occurring and artificial porous aluminosilicates in which a generally anionic framework is balanced by cations, usually located within the solid cavities or channels, although by no means filling them. The global annual market for zeolites is several million tons and they have been phenomenally successful over a wide range of applications particularly in catalysis and separation science problems, especially in the petrochemicals industry. Key areas include adsorptive separation of hydrocarbons, purification of gases and liquids, and catalytic cracking of long-chain hydrocarbons to form more valuable short-chain homologues. Zeolites also have applications in ion exchange, particularly as a detergent additive (water softening), and the separation and extraction of gases and solvents, *e.g.* as 'molecular sieves' for dehydration of organic solvents. The general formula defined by the International Union of Pure and Applied Chemistry (IUPAC) for a zeolite takes the form:

$[A_aB_bC_c]$	$\{(Al_dM_eSi_f)O_g\}$	$(xH_2O,\ yN)$
Cations A, B, C	Framework composition	Occluded guests

Each species is also denoted by a three-letter structure code that describes the framework topology (connectivity, channel dimensionality *etc.*). Examples are given in Table 9.1; common structures of some representative zeolites are shown in Figure 9.6.

Table 9.1 Characteristics of some common zeolite framework topologies.

Structure type code	Type of material: Name	Type of material: Formula	Framework composition	Channel system	Pore opening	Cage	Comments
AFI	$AlPO_4$-5	$Al_{12}P_{12}O_{48}$	$AlPO_4$-based High silica	1D	12-rings 7.3 Å	None	
FAU	Faujasite	$M_{29}[Al_{58}Si_{134}O_{384}]\cdot 240H_2O$	Aluminosilicate	3D	12-rings	*fau*	ABC stacking of puckered sodalite cage layers
		(M = Na_2, Ca, Mg)	High silica		7.4 Å	*sod*	
			$AlPO_4$-based			d6R	
LTA	Linde type A	$\{Na_{12}[Al_{12}Si_{12}O_{48}]\cdot 27H_2O\}_8$	Aluminosilicate	3D	Eight-rings	*sod*	
			High silica		4.1 Å	α	
			$AlPO_4$-based				
			$GaPO_4$-based				
MEL	ZSM-11	$Na_n[Al_nSi_{96-n}O_{192}]\cdot 16H_2O$	High silica	3D	Elliptical	None	Straight channels
		(n < 16)			10-rings 5.5 Å (mean)		
MFI	ZSM-5	$Na_n[Al_nSi_{96-n}O_{192}]\cdot 16H_2O$	High silica	3D	Elliptical	None	One straight and one zigzag channel
		(n < 27)			10-rings 5.5 Å (mean)		
SOD	Sodalite	$Na_6[Al_6Si_6O_{24}]\cdot 2NaCl$	Many combinations of Al, Si, P, Ga, Be, As and Zn	None	6-rings only 2.8 Å	*sod*	ABC stacking of six rings

Zeolites are generally regular crystalline materials, although defects such as non-bridging oxygen atoms, vacant sites or large pores are common, and often contribute to the reactivity of the materials. Silicon is the key element in the zeolite framework, with aluminium, as the AlO_4^- anionic fragment, most easily substituted within the neutral SiO_4 sites. In every case the oxygen atoms are bridging. A wide range of other TO_4 species (termed the *primary building units*) may also be included (T = tetrahedral centre such as Ge, Ga, P, As *etc.*). In zeolites, Al/Si ratios are known from one to infinity, which corresponds to a minimum requirement that there should be no Al–O–Al bonds anywhere in the structure; only Al–O–Si and Si–O–Si are stable. Based on their aluminium to silicon ratio, zeolites are usually divided into two broad categories:

1. Zeolites with low or medium Si/Al ratio (Si/Al < 5).
2. Zeolites with high Si/Al ratio (5 < Si/Al).

Materials with very high Si/Al ratios (tending to infinity) are called all-silica molecular sieves, zeosils or porosils. If any aluminium is present, non-framework cations such as alkaline or alkaline earth metals

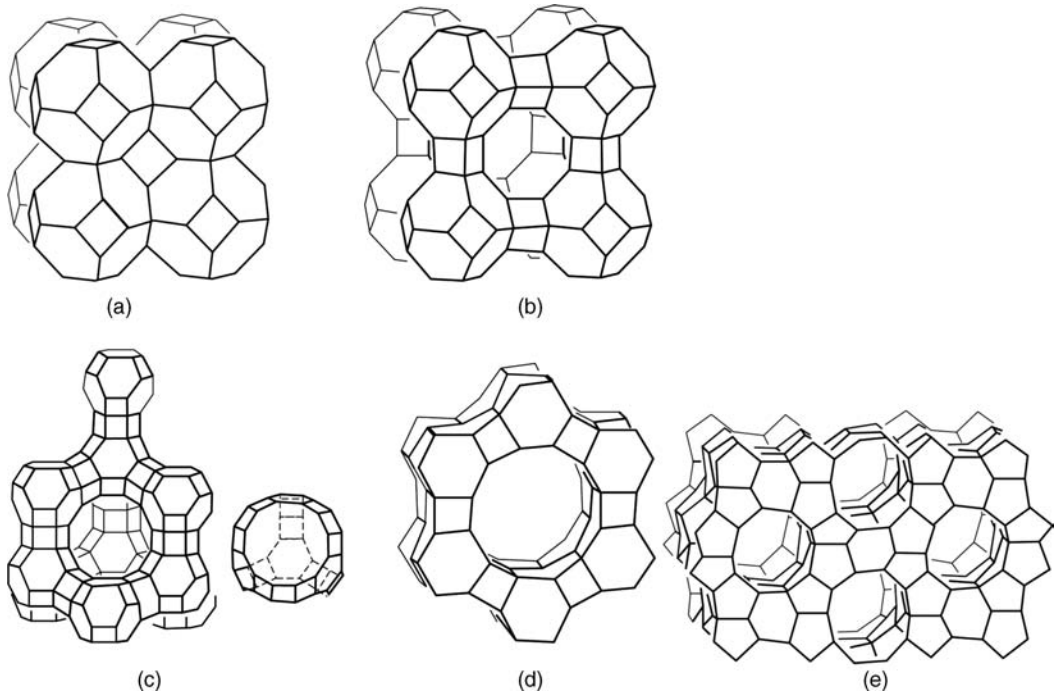

Figure 9.6 Topologies of zeolite structure types. (a) Sodalite; (b) Linde type A; (c) faujasite (zeolite X and Y); (d) $AlPO_4$-5; and (e) ZSM-5. The vertices represent the positions of AlO_4^- or SiO_4 tetrahedra while straight lines represent Si–O–Si or Si–O–Al linkages. (Reproduced with permission from [5]).

or organic tetraalkyl or tetraarylammonium ions are incorporated within the pores. Neutral organic molecules or solvent molecules and water may also be present depending on the synthesis method. The smaller cations may be exchanged in ion-exchange processes, while the organic species may be transformed into protons by calcination (heat treatment at about 500 ºC).

About 60 naturally occurring zeolites are known, of which bikitaite, $Li_2[Al_2Si_4O_{12}]\cdot 2H_2O$, heulandite, $Ca_4[Al_8Si_{28}O_{72}]\cdot 24H_2O$ and faujasite, $(Na_2, Ca, Mg)_{29}[Al_{58}Si_{134}O_{384}]\cdot 240H_2O$, are examples. The first naturally occurring zeolite, stilbite ($NaCa_2Al_5Si_{13}O_{36}\cdot 14H_2O$), was discovered by the Swedish mineralogist Crønsted about 250 years ago who found that the new mineral released water on heating, hence its name from the Greek *zeo* (to boil) and *lithos* (stone). Many of the more important zeolites, such as ZSM-5 used in the petrochemicals industry for gasoline production, are synthetic, however. Recent template syntheses using surfactants have given access to very interesting mesoporous (intermediate pore size) materials such as MCM-41 and MCM-48, which have much larger cavities than the traditional microporous materials. ZSM and MCM stand for Zeolite Socony Mobil and Mobil Catalytic Material respectively. They form part of a large series of three-letter code descriptions for particular series of materials, particularly those of industrial importance, which have a historical basis, but are still in common usage. A full listing is given on the web site of the International Zeolite Association cited at the beginning of this section. Much of the usefulness and chemistry of zeolites arises as a consequence of the presence of channels and cavities in the structures, which include metal cations (which counterbalance the charge of the anionic framework), water and a vast range of other guests. The beauty of zeolites is that the aluminosilicate cages are sufficiently robust that guest species may enter and leave the channels with no disruption of the host structure. As a result, zeolites are used as 'molecular sieves', separating catioic and molecular guests on a size or adsorption-selective basis, and as reaction vessels for high selective intrachannel and intracavity reactions.

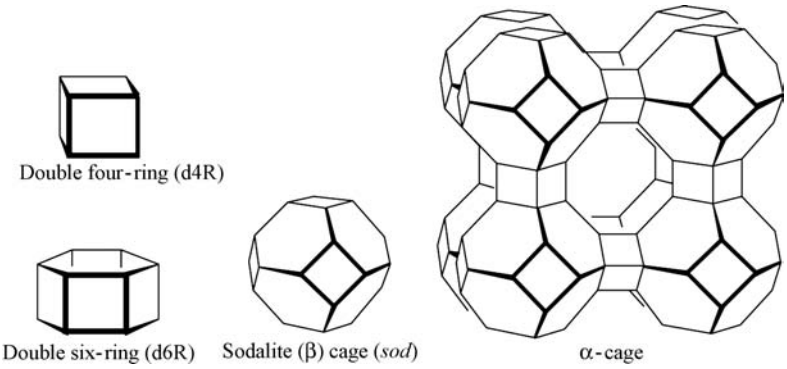

Figure 9.7 Zeolite cage structures incorporated as *secondary building units*.

In general the tetrahedral primary building units form common structural features termed *secondary building units* (SBU – some examples are shown in Figure 9.7) that are linked together in different ways to give the overall zeolite structure. The inclusion chemistry of zeolites depends very much on the channel and pore size and on the size of the windows giving access to those solid state cavities. In the case of sodalite, the β-cages (Figure 9.7) are accessible only through four- and six-membered rings (that is comprising four or six tetrahedral atoms with their associated oxygen linkers) that are not large enough to admit the vast majority of guest species. In contrast, the Linde type A (LTA) topology, while still based on sodalite cages, contains additional double four-ring spacers. This results in α-cages accessible by eight-rings and giving the material an overall three-dimensional channel structure. Extending the structure still further, in the faujasite type, sodalite cages are arranged in a tetrahedral fashion, exactly like the carbon atoms in diamond, joined by double six-rings. The result is the faujasite cage (*fau*), which comprises a three-dimensional 12-ring channel system. The framework is highly porous and ideal for a number of inclusion catalytic purposes.

In contrast to the SOD, LTA and FAU topologies, ZSM-5 and ZSM-11 are not based on the sodalite motif. They are complex structures with 10-ring aperture channels based on the 'six-ring wrap' motif in which the channel walls are made of a sheath of fused six-rings. The only difference between the two substances is the occurrence of an inversion centre in ZSM-5 and a mirror plane in ZSM-11. This results in one straight and one zigzag channel in ZSM-5 (Figure 9.8) and entirely linear channels for ZSM-11. The AFI type, typified by $AlPO_4$-5, is also based on channels. In pure aluminophosphate zeolites, the Al^{3+} and PO_4^{3-}components strictly alternate to give a neutral cage framework and so there are only even-membered rings. The pore system is based on a one-dimensional channel with 12-ring openings.

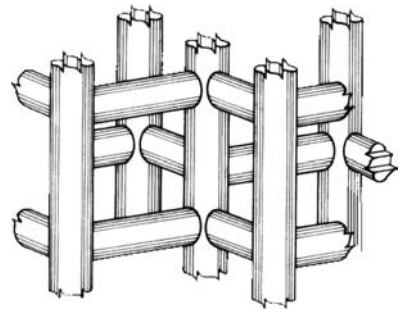

Figure 9.8 Linear and zigzag channels in ZSM-5.

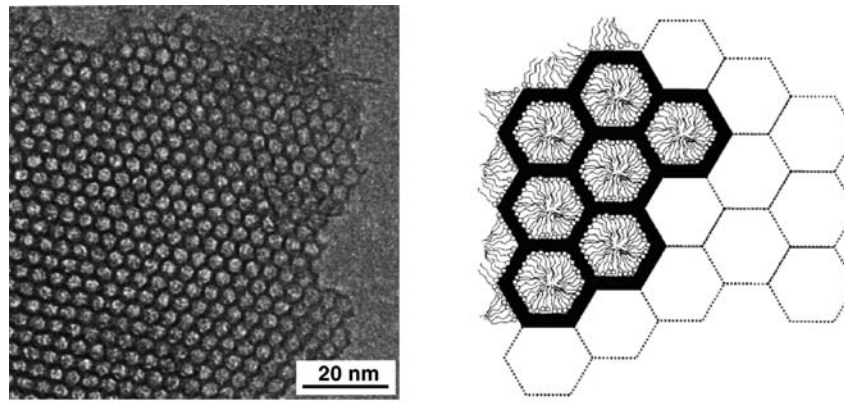

Figure 9.9 (a) High resolution TEM image of calcined MCM-41 showing the hexagonal mesoporous structure, (b) schematic diagram of how the mesopores are templated using a surfactant (reprinted with permission from [6] © 2000 American Chemical Society).

The zeolites shown in Table 9.1 are all examples of microporous materials, so called because of their relatively small pore dimensions. In 1992, the M41S family of zeolites, of which MCM-41 and MCM-48 are members, were reported by Mobil. These species are templated by surfactant molecules such as alkyl trimethylammonium salts $NRMe_3^+$ ($R = C_nH_{2n+1}$; $n = ca.\ 12 - 22$) that form micelles in solution (Section 13.2.1), templating the formation of very large pores (mesopores) with the pore size depending on the length of R.[6] Zeolite MCM-41 has a one-dimensional hexagonal arrangement of open channels of dimensions 15–100 Å, readily observed by transmission electron microscopy, Figure 9.9. MCM-48 has a three-dimensional arrangement of pores about 30 Å in diameter, in a cubic arrangement. These mesoporous materials have opened up a new field in 'expanded' zeolite compounds over the past 15 years or so. Other approaches to these larger pore compounds include the preparation of delaminated zeolites from zeolite precursors and synthesis of pillared layered materials with spaced zeolite layers.[7]

9.2.2 Synthesis

In order to prepare zeolites of well-defined structural type, templating materials must be used which determine the pore size distribution. The overall mechanism of zeolite formation is thought to involve the gradual replacement of water of hydration about the templating cation by silicate or aluminosilicate units. Thus, the pore size is determined by the dimensions of the cation, subject to the formation of an at least metastable framework. Some examples of cations and the zeolite types templated are given in Table 9.2. A wide range of other factors such as the crystal deposition kinetics and Si/Al ratio must also be controlled. As a result, zeolite synthesis is commonly carried out in a solid gel phase, in which the framework building species are supplied continuously at a controlled rate by continuous dissolution. A general synthesis scheme is shown in Figure 9.10.

Control of pH is critical in the determination of the Si/Al ratio. As the pH increases, the ability of the silicate to condense decreases because of a decrease in the amount of Si–O^-species relative to Si–OH. The anionic form is necessary in order for the initial nucleophilic attack to take place. In contrast, the condensation rate of $Al(OH)_4^-$ remains constant and so aluminium-rich zeolites crystallise preferentially at high pH and vice versa. Zeolite synthesis also depends on a wide range of experimental parameters, including concentrations and degree of supersaturation, the source of the framework materials, solvent

Table 9.2 Templating cations and the resulting zeolites.

Cations	Zeolite type
Na^+	Sodalite
$Na^+ + NMe_4^+$	Faujasite, sodalite, zeolite-A (LTA)
$Na^+ + NPr_4^+$	ZSM-5
Na^+ + benzyltriphenylammonium	ZSM-11
Na^+ + [15]crown-5	High-silica faujasite
$C_nH_{2n+1}Me_3N^+$ (n = 8–16)	MCM-41

(sometimes alcohols or glycols are used), gel dissolution rate, ageing, addition of seed crystals, temperature, agitation time, and pressure. The ideal parameters have been determined quite precisely by experimentation and zeolites may be prepared readily in large quantities.

9.2.3 MFI Zeolites in the Petroleum Industry

Marcilly, C., 'Zeolites in the petroleum industry', in *Encyclopedia of Supramolecular Chemistry*, Atwood, J. L., Steed, J. W., eds. Marcel Dekker: New York, 2004; Vol. 2, *pp.* 1599–1609.

The MFI class of channel zeolites, of which ZSM-5 is a member, are of enormous importance in the petrochemicals industry because of their shape-selective adsorption and transformation properties. The most well-known example is the selective synthesis and diffusion of *p*-xylene through ZSM-5, in preference to the *o*- and *m*-isomers. Calcined zeolites such as ZSM-5 are able to carry out remarkable transformations upon normally unreactive organic molecules because of 'super-acid' sites that exist

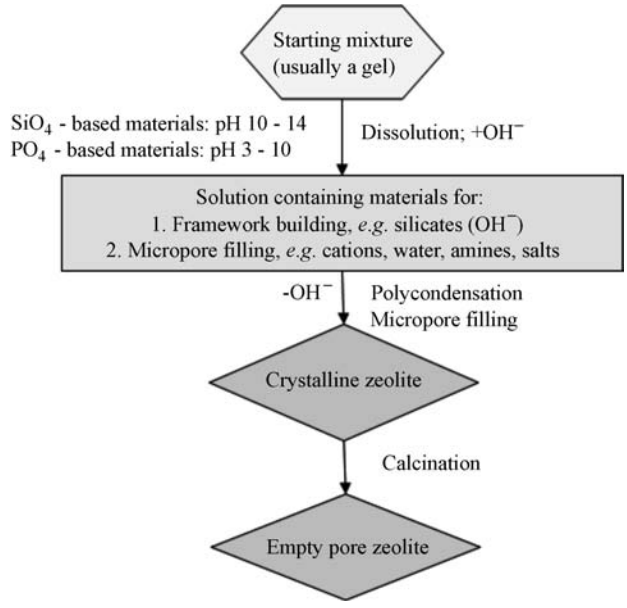

Figure 9.10 Schematic diagram illustrating zeolite synthesis in the presence of a mineraliser (*e.g.* OH^-) in aqueous phase.

within the zeolite pores. In calcined zeolites, the negative charge of the framework is balanced only by protons, which reside either upon defect sites or on bridging oxygen atoms. In the empty zeolite cavity, the proton is unsolvated and is therefore extremely reactive. This has the result that even very weak bases such as aromatic hydrocarbons, and even *n*-alkanes and waxes, are protonated as they diffuse through the zeolite channels, forming reactive carbocations that may readily rearrange, forming a mixture of products. Intracavity synthesis of xylenes is carried out by reaction of toluene with methanol. The zeolite acidity results in electrophilic aromatic substitution of the aryl ring to give a mixture of *o*-, *m*- and *p*-xylenes, which are in a state of equilibration within the zeolite medium. Crucially it is only the *para* isomer that is able to diffuse readily through the zeolite channel, however, because of its linear, thread-like shape. The more bulky *ortho* and *meta* isomers are much less mobile in the zeolite interior, and hence are much more likely to reisomerise, forming an additional statistical amount of *p*-xylene, which again diffuses away. In this way, zeolites such as ZSM-5 are highly *para*-selective. This property is known as *diffusion selectivity*. In fact, the *para* isomer diffuses about 14 times faster than the *o*-isomer and about 1000 times faster than *m*-xylene (Figure 9.11a)

The zeolites' high acidity is also of crucial importance in the production of gasoline *via* the 'M-forming' process. In gasoline, linear *n*-alkanes are relatively undesirable compared to their branched counterparts because of their lower octane numbers. Separation of linear and branched materials increases the value of the gasoline. Better still, if linear materials can be converted into branched species,

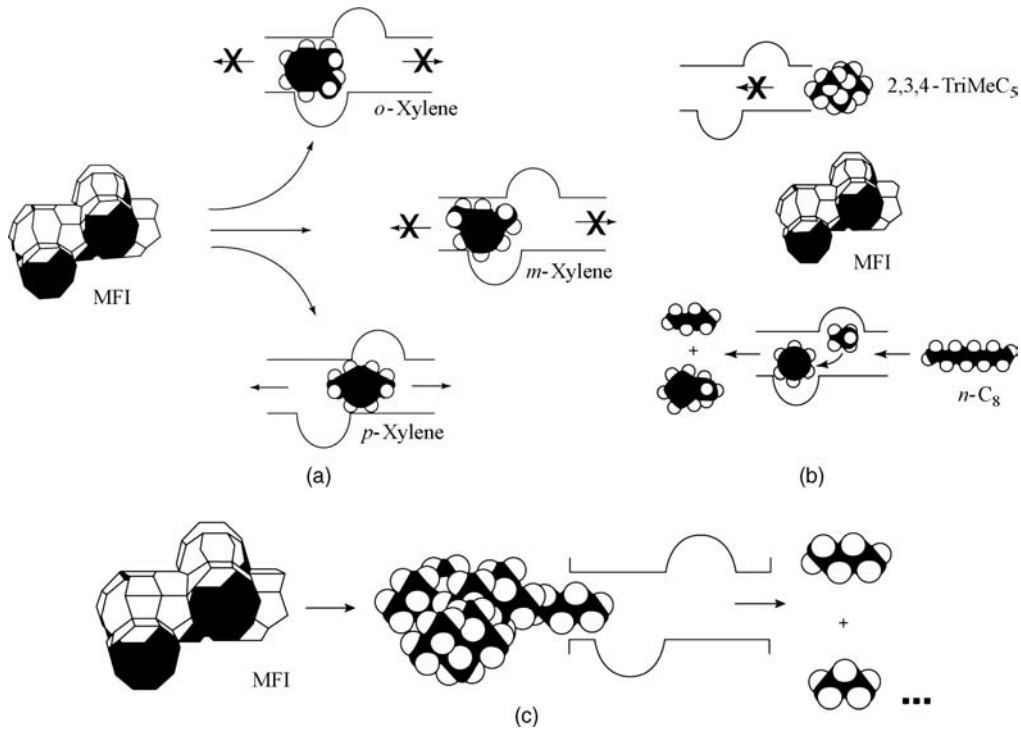

Figure 9.11 (a) Diffusion shape selectivity in xylene isomerisation. (b) The M-forming process for gasoline upgrading by MFI-type zeolites; high-octane compounds such as 2,3,4-trimethylpentane are prevented from reacting by both transition state and diffusion selectivity; *n*-alkanes penetrate into the channels and are cracked; aromatics are alkylated with the light fragments from cracking. (c) Wax components are cracked into gasoline and liquid petroleum gas. (Reproduced with permission from [8]).

significant profit may be generated. Highly branched alkanes such as 2,3,4-trimethylpentane diffuse very slowly into the ZSM-5 channels. Furthermore, even if they do find themselves within the zeolite, the primary mechanism for alkane isomerisation involves hydride transfer to a zeolite cationic site. The transition state for this reaction is highly bulky and, as a result, only linear alkanes are able to undergo reaction. This is known as *transition state selectivity*. Both transition state selectivity and diffusion selectivity, therefore, result in valuable branched hydrocarbons being unchanged by the zeolite. On the other hand, linear species such as *n*-octane diffuse readily into the zeolite and react with the acid sites, resulting in their catalytic cracking to lighter fractions, readily separated from the mixture. Aromatics are alkylated by the cracking fragments and contribute to the gasoline product, resulting in little volume loss. Since the carcinogen, benzene, is the most reactive there is a desirable lowering of the benzene: toluene ratio in the product (Figure 9.11b).

Other larger zeolites of the FAU type are used in the cracking of long-chain waxes and paraffins, which are of low value because of their viscosity. The products of this process are gasoline and liquid petroleum gas, which is treated further with MFI-type zeolites as detailed above (Figure 9.11c).

9.3 Layered Solids and Intercalates

9.3.1 General Characteristics

O'Hare, D., 'Inorganic intercalation compounds', in *Inorganic Materials*, D.W. Bruce and D. O'Hare (eds), J. Wiley & Sons, Ltd: Chichester, 1996, 171–254.

Layered solids include materials such as graphite, cationic and anionic clay minerals, metal phosphates and phosphonates, and a range of other inorganic and coordination compounds. The first report of their occurrence seems to be the production of porcelain by the Chinese around AD 600–700. This occurs by the intercalation, or inclusion, of alkali metal ions in naturally occurring layered minerals such as feldspar or kaolin. A layered solid is characterised by a two-dimensional sheet arrangement in which the components of the sheet interact covalently (or are otherwise strongly bound), while the interactions from one sheet to the next are of a weak type, commonly van der Waals interactions. Some of the characteristics of layered solids are summarised in Figure 9.12, while examples of various classes of layered material are given in Table 9.3.

The layered arrangement makes these materials very interesting from the point of view of host–guest behaviour because ionic or molecular guest species may be inserted between one layer and another causing the layers to expand or swell. Guest intercalation is generally reversible, and it is an important characteristic of layered solids that, rather like zeolites, they can retain their layered host structure

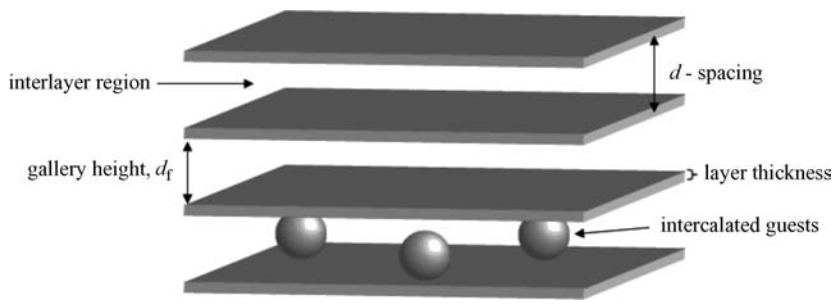

Figure 9.12 Characteristics of layered solids.

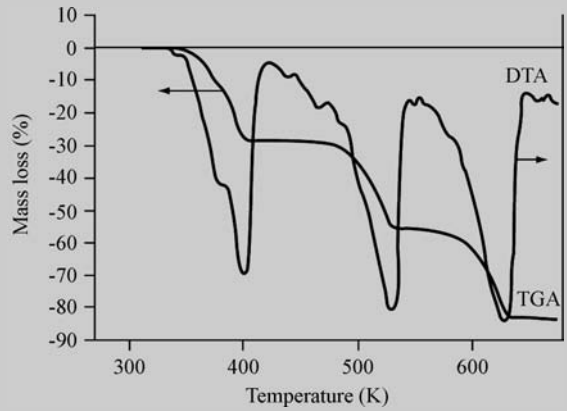

Figure 9.22 DTA–TGA trace for $Ni(NCS)_2(4\text{-Phpy})_4 \cdot 4C_6H_6$ showing the endothemic loss first of benzene and then the 4-phenylpyridine ligands in two distinct stages. (Reprinted with permission from IUCr).

9.5 Coordination Polymers

9.5.1 Coordination Polymers, MOFs and Other Terminology

Yaghi, O. M., O'Keeffe, M., Ockwig, N. W., Chae, H. K., Eddaoudi, M. and Kim, J., 'Reticular synthesis and the design of new materials', *Nature* 2003, **423**, 705–714.

The term *coordination polymer* very broadly encompasses any extended structure based on metal ions linked into an infinite chain, sheet or three dimensional architecture by bridging ligands, usually containing organic carbon. More recently the term *metal organic framework* (MOF) has entered the literature. A metal organic framework is a kind of coordination polymer that is a three-dimensional, crystalline solid that is both robust and porous. The organic bridging ligands within MOFs are generally subject to some kind of synthetic choice and hence coordination polymers involving simple ligands such as cyanide are not generally considered MOFs. The chemistry of MOFs has benefited greatly from the introduction of concepts from zeolite chemistry, particular the secondary building unit (SBU) and there are now MOF frameworks with significant structural robustness with pores in the mesoporous domain (see Section 7.9 for an explanation of pore size classification). Another powerful concept is *reticular synthesis* (the synthesis of periodic repeating nets) leading to *isoreticular expansion* and *decoration*. Isoreticular expansion means the increasing of the length of a spacer while retaining the same network topology. Thus an isoreticular MOF (IRMOF) is (usually) an expanded version of a previously known MOF. This expansion generally leads to larger pore size and is a feature of the control allowed by synthetically designable building blocks. Decoration means replacing a vertex within a net with a series of vertices. In general the entire field of coordination polymer chemistry is of tremendous current interest, in the main because of the tremendous diversity (and hence tunability) and scope for design in the construction of new materials that are hybrids between metals and/or metal clusters and organic ligands within the context of designer materials chemistry. It is fair to say that the scope for the application of MOFs in gas separation and storage, particularly as

hydrogen storage materials (Section 7.9) is one of the principal driving forces in current research endeavour. However there are many other uses and areas of interest in coordination polymer chemistry. These include magnetism and magnetic spin crossover behaviour, non-linear optical activity, catalysis and negative thermal expansion. We will look briefly at each of these areas in the following sections. Before embarking upon a necessarily concise description of the metals, SBUs, ligands and structures encountered in modern coordination polymer chemistry we list below some useful terms that we will be encountering along the way.

- *Reticular*: (adjective) having the form of a (usually periodic) net.
- *Isoreticular*: Based on the same net (having the same topology).
- MOF-*n*: Metal-organic framework (where *n* is an integer assigned in roughly chronological order of discovery, *e.g.* MOF-5).
- IRMOF-*n*: Isoreticular MOF (with *n* an integer referring to a member of the series).
- *Interpenetration*: A term used to describe the mutual intergrowth of two or more networks in a structure where the networks are physically but not chemically linked.
- *Expansion*: Increasing the spacing between vertices in a network.
- *Decoration*: Replacing a vertex in a net by a group of vertices.
- SBU: Secondary building unit in the context of coordination polymer network synthesis (reticular chemistry) refers to the geometry of metal coordination cluster fragments units as defined by the points of extension (such as the carboxylate C atoms in most carboxylate MOFs).
- *Supramolecular isomerism*: the existence of more than one type of network superstructure for the same molecular building blocks (Section 8.5.2).

9.5.2 0D Coordination Clusters

There exist a vast number of discrete, polymetallic coordination clusters both of the metal-metal bonded type and linked by a tremendous variety of bridging ligands, notably carboxylates. Such compounds are not coordination polymers but oligomers and hence can be more soluble, more well-defined and easier to characterise than coordination polymers, for which they can serve as useful model systems. We will discuss discrete, self-assembled complexes of semi-protected metal ions that act as hosts in solution or as 3D capsules in the next chapter and we will not cover these systems in detail here except to note in passing a couple of examples that are of particular interest. One particularly prominent cluster is Mn_{12}-acetate,[19] the mixed-valence compound $[Mn^{III/IV}{}_{12}O_{12}(CH_3CO_2)_{16}(H_2O)_4]$ studied intensively since the early 1990s. This discrete cluster is a disk-like cluster with a cube-shaped $Mn^{IV}{}_4O_4$ core bridging to either Mn(III) ions, with bridging acetate at the periphery of the disk, Figure 9.23. The compound was one of the first and still most significant *single molecule magnets*. It has an $S = 10$ ground state (S = total spin quantum number, corresponding to 20 unpaired electrons) and there is a significant barrier to magnetisation relaxation meaning that this molecule is a prototype component of a 'spin computer' because it can store digital information according to its magnetisation state. A large number of comparable clusters have since been discovered.[20]

Also of interest in the context of supramolecular chemistry is recent work on very large entirely inorganic spherical capsules based on the $(pentagon)_{12}(linker)_{30}$ type such as the polyoxomolybdate $[P_{12}\{Mo_2O_4(MeCO_2)\}_{30}]^{42-}$ (Figure 9.24, where P = the pentagonal cluster $\{(Mo)Mo_5O_{21}(H_2O)_6\}^{6-}$). These structures are examples of a general series of large, polymetallic cyclic structure obtained from

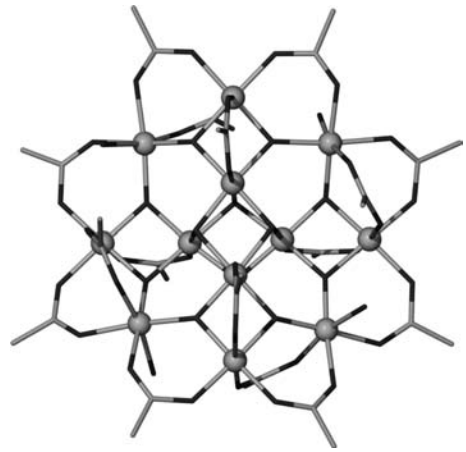

Figure 9.23 Structure of Mn_{12}-acetate, a single molecule magnet (Mn ions shown as spheres).[19]

molybdenum 'blues' – partially reduced solutions of Mo(VI) oxides in the presence of templating agents. The characteristic blue colour arises from the presence of delocalised electrons. In the case of the spheres these entirely synthetic, abiotic containers can function as a kind of artificial biological cell (or a nano-chromatograph for the separation of metal ions).[21] The capsule size and shape can be tailored by careful choice of conditions and the largest such hollow sphere comprises 368 Mo atoms and has an internal cavity 2.5 nm wide and 4 nm long, containing about 400 structured water molecules in a confined environment. Metal cations are able to selectively diffuse in and out of the holes created by the carboxylate substituents with a significant dependence on the ability of the water confined within the capsule to coordinate to the cation. The confined environment of this 'inorganic cell' exhibits some remarkable properties while the polyoxomolybdate cell wall exhibits some features in common with cation transport through biological ion channels (*cf.* Section 2.2). The adaptation of the confined

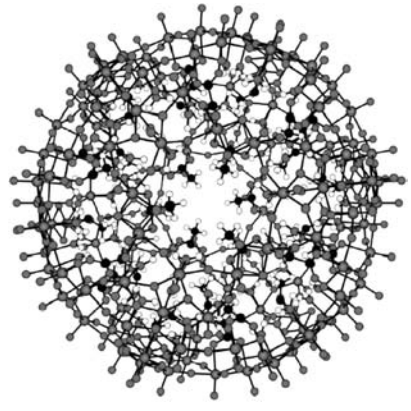

Figure 9.24 The polyoxomolybdate nanocluster $[P_{12}\{Mo_2O_4(MeCO_2)\}_{30}]^{42-}$ (P = $\{(Mo)Mo_5O_{21}(H_2O)_6\}^{6-}$) that behaves as an artificial cell, showing the pore opening in the centre (reprinted from [21] with permission of Elsevier).

structured water to the ingress of metal ions suggests insights into the way in which a biological cell converts an incoming chemical signal into a response.

9.5.3 1D, 2D and 3D Structures

Moulton, B. and Zaworotko, M. J., 'From molecules to crystal engineering: Supramolecular isomerism and polymorphism in network solids', *Chem. Rev.* 2001, **101**, 1629–1658.

The transition from discrete complexes to coordination polymers can be seen as a logical progression as we change from semi-protected metal ions (*i.e.* those in which one face is blocked off by a spectator ligand such as ethylene diamine (en), acetylacetonate (acac) or [9]ane-S_3) to naked ones, and in doing so increase their potential for network connectivity. For example, using linear pyridyl type ligands such as 4,4′-bipyridyl (bpy) we can identify a progression from a 0D box as exemplified by $[\{Pd(en)(\mu\text{-bpy})\}_4]^{8+}$,[22] in which two cis-related sites are available on the metal centre, to a 1D chain-type coordination polymer, $[Zn(acac)_2(\mu\text{-bpy})]_n$,[23] in which two *trans* sites are available to propagate the chain, to a 2D grid using axially protected Co(II) with 4 equatorial sites, $[Co(bpy)_2(CF_3CO_2)_2]_n$,[24] and finally a 3D network structure based on the related pyrazene ($N_2C_4H_4$) with the rare octahedral Ag(I), $\{[Ag(pyrazene)_3](SbF_6)\}_n$ using unprotected metal ions (Figure 9.25).[25]

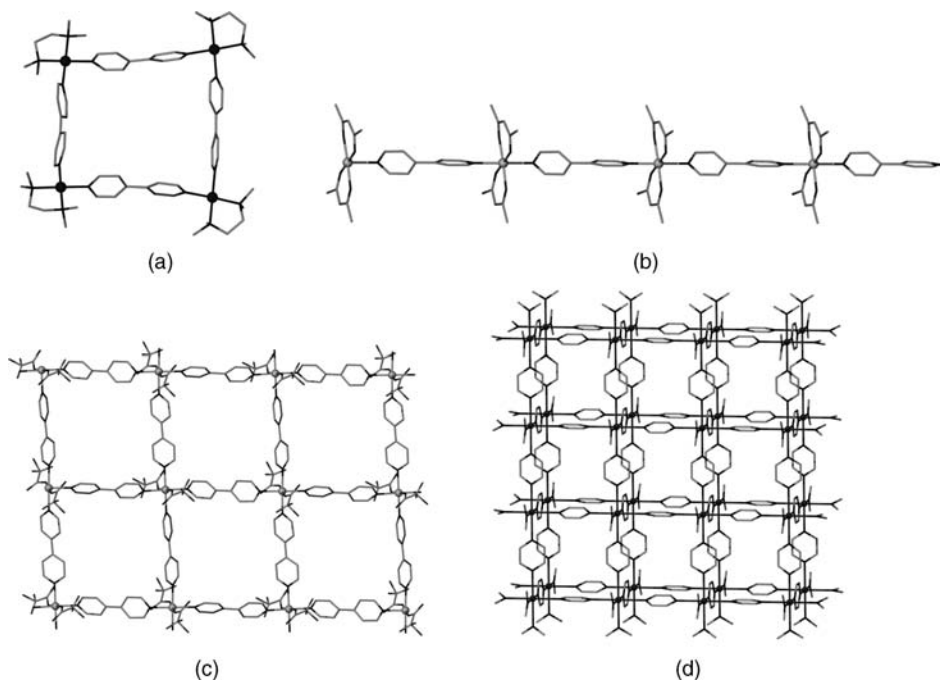

Figure 9.25 Progression from 0D discrete self-assembled complexes to 1D, 2D and 3D architectures as the degree of 'protection' around the metal centre from spectator ligands is decreased, as exemplified by 4,4′-bipyridyl complexes (a) $[\{Pd(en)(\mu\text{-bpy})\}_4]^{8+}$,[22] (b) $[Zn(acac)_2(\mu\text{-bpy})]_n$,[23] (c) $[Co(bpy)_2(CF_3CO_2)_2]_n$,[24] and (d) the pyrazene complex $\{[Ag(pyrazene)_3](SbF_6)\}_n$.[25]

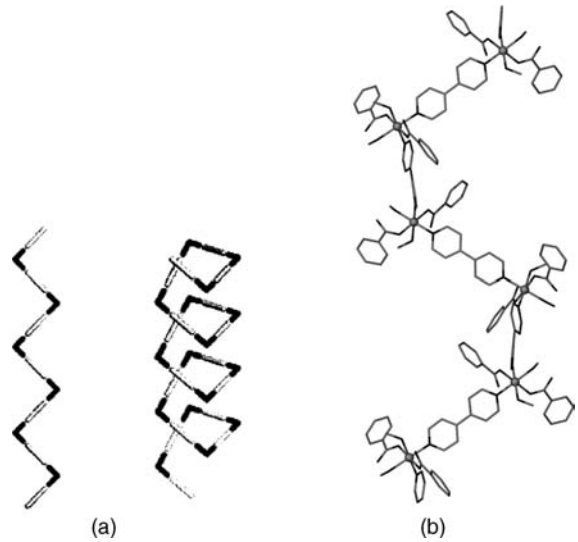

Figure 9.26 (a) zig-zag and helical supramolecular isomers of 1D chains made up of a linear spacer (light grey) and a *cis* metal centre (black) (reprinted with permission from Section Key Reference © 2001 American Chemical Society). (b) chiral helical structure of $[Ni(bpy)(benzoate)_2(MeOH)_2]$.

As we progress from 0D to networks the compounds become insoluble, but all are potentially capable of including guests depending on the lengths of the spacers, size of the nodes and degree of interpenetration.

In terms of 1D coordination polymers based on *cis* related coordination sites on a square planar or octahedral metal centre, they can adopt either zig-zag or helical chain architectures (as well as a discrete triangle, square or other box-like structure). The zig-zag and helical structures are supramolecular isomers of one another and fundamentally differ in that the helical structure is intrinsically chiral even if the building blocks that comprise it are not, Figure 9.26a. Zig-zag polymers are fairly common, while the helical structure is more unusual. A nice example of the latter is $[Ni(bpy)(benzoate)_2(MeOH)_2]$ which forms aligned helices in the solid state (Figure 9.26b) with void cavities of *ca.* 500 $Å^3$ able to accommodate nitrobenzene guests arranged in dimers. In many cases of chiral motifs within crystals both enantiomers are simultaneously present meaning that there is no overall crystal chirality. In this case, however, every individual crystal is chiral because the helices are aligned rather than antiparallel. Moreover, as we saw in Section 8.2.4, seeding may give rise to bulk chiral samples opening the possibility of chiral separations of guests.

Another kind of 1D coordination polymer is the ladder structure, this time made up of 3-connected nodes. One connector per node makes up a rung of the ladder and hence the polymer only propagates in one dimension producing a flat ribbon-like structure. With ligands like bpy the 3-connected node and bidentate nature of the ligand require a metal : ligand stoichiometry of 1:1.5 as in $[Co(bpy)_{1.5}(NO_3)_2]\cdot 2CHCl_3$ in which the chloroform guests reside in square cavities between the rungs. A good example of a simple expansion is the replacement of bpy with the extended 1,2-bi-4-pyridylethane which gives a closely related structure in which there is room for three chloroform molecules.

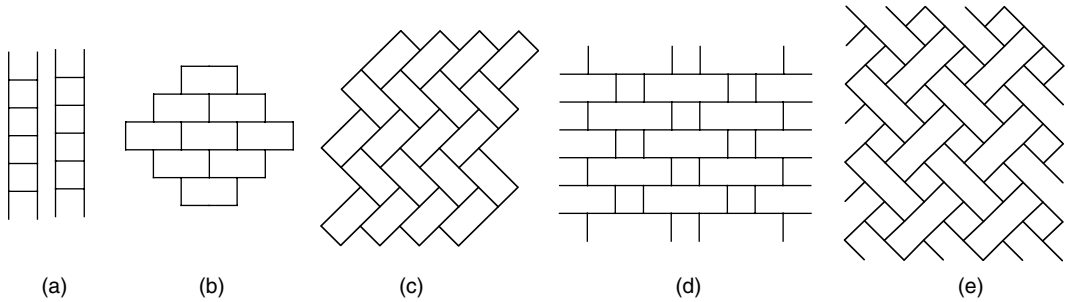

Figure 9.27 Possible 3-connected networks (a) 1D ladder, (b) 'brick wall' (c) herringbone, (d) long and short brick and (e) basket weave. The latter two networks have yet to be realised in practice.

In terms of two dimensional coordination polymers the square grid (4,4) network is very common with square planar and axially-capped octahedral metal ions, as in $[M(bipy)_2(NO_3)_2]\cdot$guest (M = Co, Ni). Various types of compound within this series exist depending on grid shape (as opposed to topology), host:guest stoichiometry and the interactions of one 2D layer with the next. 2D nets can also be produced based on 3-connected nodes. The 'brick wall' (6,3) net is one example that has been realised. Examples of the related herringbone (6,3)-net are also known but the other theoretically possible networks (Figure 9.27d and e) have not yet been realised.

A particularly novel 2D net based on pentagons (which cannot tessellate in two dimensions) is also known. The net topology is $\left(5,^{3}_{4}\right)$ in Wells nomenclature, meaning that it is composed of 3- and 4-connected nodes linked by 5-gons. The pentagons are not regular and the 2D sheets have a wave-shape to them allowing them to tessellate. Chemically the compound is of formula $[(HMTA)_3(Cu_2(\mu\text{-}O_2CCH_2CH_3)_4)_5]_n$ (HMTA = hexamethylene tetramine).[26] The 3- and 4-connected nodes are both the HMTA ligands and the spacers are the linear $[Cu_2(\mu\text{-}O_2CCH_2CH_3)]_4$ bimetallic fragments. The fact that a bimetallic cluster is involved instead of a simple metal ion is an example of the use of an SBU. The tetrahedrally disposed nitrogen atoms on HMTA give the non-planarity to the sheets with all four being involved in bonding in the 4-connected nodes. One HMTA atom is unconnected in the 3-connected nodes which act to cap the sheets, Figure 9.28.

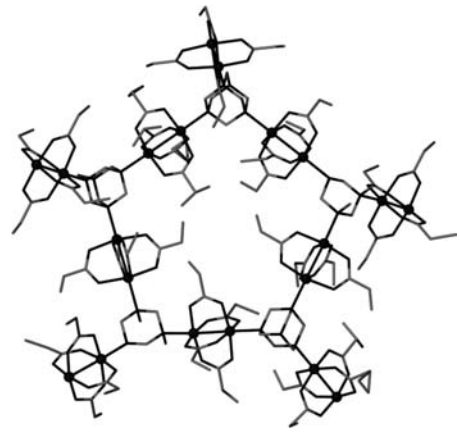

Figure 9.28 A surprising $\left(5,^{3}_{4}\right)$-net based on irregular pentagons in the structure of $[(HMTA)_3(Cu_2(\mu\text{-}O_2CCH_2CH_3)_4)_5]_n$.[26]

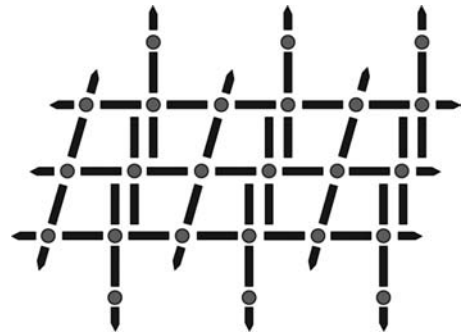

Figure 9.29 NbO framework of $[Cu(1,2\text{-bi-4-pyridylethane})_2(NO_3)_2]_n$. (Reproduced with permission of The Royal Society of Chemistry).

Three-dimensional networks offer the most scope for the construction of robust frameworks and also in some ways are the most subject to design by the crystal engineer/materials chemist. For example a tetrahedral node and a linear spacer should give a diamondoid network and indeed diamondoids account for very many 3D networks. Similarly octahedral nodes and linear spacers should, sterics allowing, give an α-Po structure. Often steric constraints and the individual shape of metals and ligands cause surprises, however. As we will see a wide variety of other 3D structures are known, either synthesised by design or more commonly, serendipitously. For example the reaction of 1,2-bi-4-pyridylethane with with Cu(II) forms a surprising network $[Cu(1,2\text{-bi-4-pyridylethane})_2(NO_3)_2]_n$ (Figure 9.29). Cu(II) is a d^9 metal ion and exhibits a strongly Jahn–Teller distorted ground state geometry in which the octahedral metal centre exhibits much longer bonds to the axial ligands (nitrate), which protrude into the grid cavities, than the bipyridyl ligands. It is unclear why Cu(II) should adopt the NbO structure with this ligand in which the equatorial plane of the metal ion is rotated through 90° compared to two of its four nearest neighbours, but the difficulty in filling the larger cavities engendered by the expanded bipyridyl ligand is a possible reason. The cavities are also filled by twofold interpenetration and still exhibit 11 × 11 Å cavities filled by benzene and methanol guest molecules. In general the dimensionality and shape of the ligand plus the dimensionality of the *free coordination sites* on the metal or fragment such as an SBU should determine the network connectivity and dimensionality, Figure 9.30.

3D networks based on the lanthanides with their high coordination numbers (typically 7–11) are less predictable than those based on transition metals and the high oxophilicity of the lanthanide(III) ions means that they do not bind strongly to ligands such as pyridine derivatives. As a result lanthanide coordination networks are less common in the literature; however, they represent tremendous potential in terms of ever more complex topologies.

Another key factor in coordination polymer design is charge balance in the structure. Structures in which neutral ligands link together charged metal ions must involve some kind of counter ion to give overall electrical neutrality. Typically non-coordinating anions such as BF_4^-, PF_6^- and $CF_3SO_3^-$ are common. These counter-anions (or in the more unusual case of anionic frameworks, counter cations) cannot be removed from a structure because of the very high strength of electrostatic forces even if they are apparently in a stack that resembles a channel (*cf.* 'virtual porosity', Section 9.1.3) and hence they fill the framework, reducing the tendency towards interpenetration or guest inclusion. They also can play a role in templating the observed shape and network topology. Charge neutral frameworks *e.g.* with divalent metals and dicarboxylate anions offer the greatest scope for overall porosity but can be difficult to synthesise because of the stronger metal-ligand bonds.

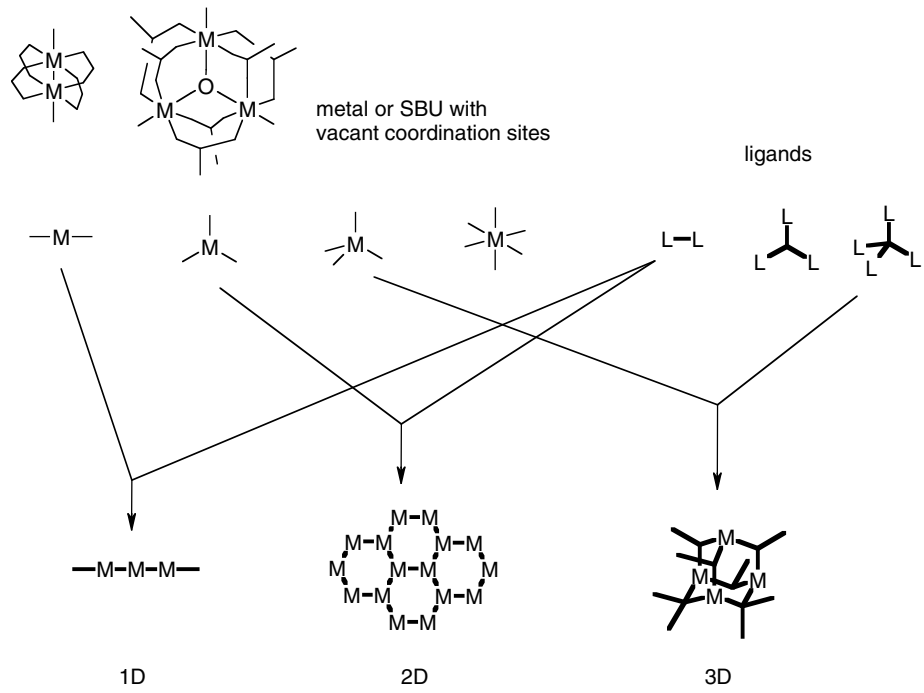

Figure 9.30 The dimensionality of the coordination polymer is dependent upon the connectivity and shape of the ligands and the distribution of the vacant coordination sites on the metal or SBU.

9.5.4 Magnetism

Batten, S. R., Murray, K. S., Structure and magnetism of coordination polymers containing dicyanamide and tricyanemethanide. *Coord. Chem. Rev.* 2003, **246**, 103–130.

The first true coordination polymer ever isolated was Prussian blue, an intensely coloured blue compound produced accidentally by a painter and dye maker Heinrich Diesbach in Berlin in 1704.[28] This material is an α-Po network of formula $Fe(III)_4[Fe(II)(CN)_6]_3 \cdot nH_2O$ (n = 14–16). The iron ions are

Figure 9.31 The rutile structure α-M(**9.5**)$_2$ Metal atoms are shown in black, nitrogen atoms in grey, carbon in white (reproduced from Section Key Reference with permission from Elsevier).

bridged by the CN^- ligands to give a cubic, three-dimensional structure. The blue colour comes about as a result of intervalence charge transfer interactions between the Fe(III) and Fe(II) ions, mediated by the short, multiple bonded cyanide ligands. Prussian blue has a long history as a pigment in monochrome printing processes, for example – its use in architecture is where the term 'blueprint' originates. It is also electrochromic, changing colour from blue to colourless upon reduction, it undergoes spin crossover (a change of spin state between low spin and high spin in response to changes in temperature or upon irradiation) and inclusion of other metals such as vanadium or chromium within the Prussian blue structure results in room temperature magnetic properties with proposed applications in areas such as data storage.

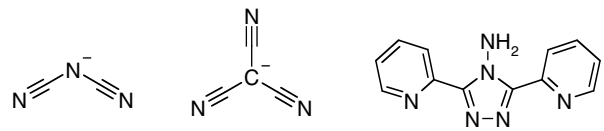

9.5 **9.6** **9.7**

Inspired by the cyanide bridges in Prussian blue, a range of polynitrile ligand have been developed such as dicyanamide $N(CN)_2^-$ (**9.5**) and tricyanomethanide $C(CN)_3^-$ (**9.6**) and used in the construction of magnetic coordination networks. Binary compounds α-M(**9.5**)$_2$ form an isostructural series (M = Cr, Mn, Fe, Co, Ni, Cu) which have a single rutile-like network (rutile is TiO_2) that involves $\mu_{1,3,5}$-bridging (*i.e.* coordination through all three nitrogen atoms) of the dicyanamides making them 3-connecting centres, while the metals are all 6-connecting with an octahedral geometry. In each case the individual metal ions have unpaired electrons and the dicyanamide ligands mediate spin-spin interactions between then resulting in different kinds of long-range magnetic order, namely ferromagnetism (parallel ordering of spins) in the case of Co, Ni and Cu while the Cr, Mn and Fe compounds are canted-spin antiferromagnets (antiparallel ordering of spins but with a net magnetic moment because the canting results in incomplete cancellation).

The discrete, mononuclear compound [Fe(**9.5**)$_2$(**9.7**)$_2$] displays the interesting phenomenon of *magnetic spin crossover*, $S = 2 \leftrightarrow S = 0$, which can be induced by both light and thermal activation.[29] Spin crossover is relatively common in Fe(II) compounds with nitrogen donor ligands and it occurs when the spin pairing energy of the *d* electrons (P) is approximately equal to the ligand field splitting energy, Δ_O that separates the upper, antibonding e_g orbitals from the lower weakly bonding t_{2g} set in octahedral transition metal compounds. Iron(II), which has six *d* electrons, at low temperatures adopts a diamagnetic ($S = 0$), low spin $(t_{2g})^6$ configuration, but at higher temperatures or when irradiated by a laser it crosses over to a metastable (large activation barrier to returning to the ground state) high spin state corresponding to the promotion to a high spin configuration with four unpaired electrons and $S = 2$, $(t_{2g})^4(e_g)^2$ (Figure 9.32). Spin crossover behaviour is also exhibited in a binuclear dicyanamide complex [Fe(L)($\mu_{1,5}$-**9.5**)Fe(L)]$^{3+}$ (where L = pentadentate polypyridyl ligand). In one particularly interesting example the magnetic spin crossover transition is linked to guest removal from an Fe(II) clathrate. The iron(II) complex **9.8** includes two molecules of diethyl ether in the solid state. Upon release of the solvent from the host crystal **9.8**·2Et_2O undergoes a single-crystal-to-single-crystal transformation to a monosolvate **9.8**·Et_2O. While the disolvate is paramagnetic (high spin) at all temperatures, the monosolvate undergoes a reversible spin crossover conversion between paramagnetism and a diamagnetic state upon cooling.[30] The implication is that the closer proximity of the metals caused by the loss of solvent mediates the spin-crossover transition.

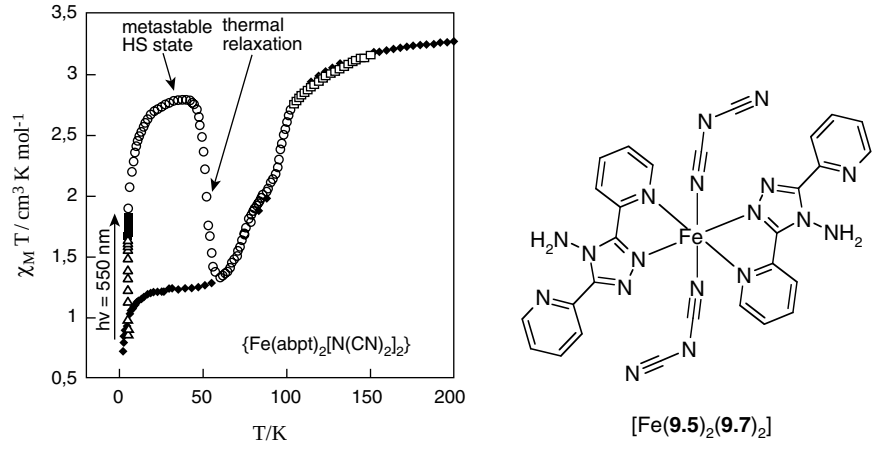

Figure 9.32 Molecular structure and magnetic spin crossover behaviour of mononuclear dicyanamide complex [Fe(**9.5**)$_2$(**9.7**)$_2$]. Filled squares correspond to cooling to just above absolute zero, resulting in a drop in magnetic susceptibility corresponding to a high-spin to low-spin transition. The sample is then irradiated promoting it back to a metastable high spin state (open triangles). The sample undergoes thermal relaxation back to the low spin state before finally a thermally induced transition back to high spin occurs between *ca.* 60 – 100 K (open circles). (Reprinted with permission from [81] © 2001 American Chemical Society).

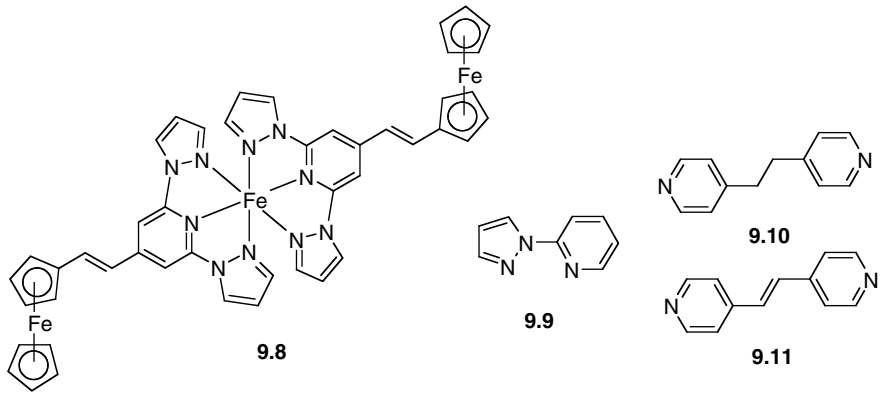

In terms of coordination polymers, in addition to Prussian blue, a range of spin crossover coordination polymers are known, many based on cyanide ligands. A series of iron(II) 1D coordination polymers have been reported, [Fe(**9.9**)$_2$(X)](ClO)$_2$·*n*EtOH (X = **9.10**, **9.11** or bpy).[31] Variable-temperature magnetic susceptibility measurements and Mossbauer spectroscopy reveal gradual spin transitions centred at *ca.* 170 – 190 K. Spin crossover in both coordination polymers and hydrogen bonded polymer materials such as [Fe(**9.5**)$_2$(**9.7**)$_2$] is of considerable interest in the context of magnetic data storage, in the same way as in the single molecule magnets discussed in Section 9.5.1.

9.5.5 Negative Thermal Expansion

Evans, J. S. O., 'Negative thermal expansion materials,' *J. Chem. Soc., Dalton Trans.* 1999, 3317–3326.

Negative thermal expansion (NTE) is a property of materials in which they become *smaller* with increasing temperature. It is a comparatively rare property and the general trend is for substances to

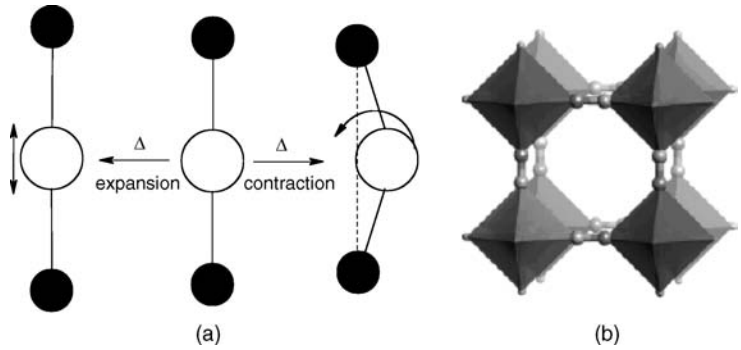

Figure 9.33 (a) Schematic illustrating the different types of vibrational motion an M-L-M bridging unit undergoes with increasing temperature. The transverse 'guitar string' motion tends to lead to NTE behaviour. Solid circle = metal, open circle = ligand such as O^{2-} or CN^{-}. (b) the structure of the Prussian Blue analogues $[M^{II}Pt^{IV}(CN)_6]$ (M = Mn, Fe, Co, Ni, Cu, Zn, Cd) as an example of the Prussian Blue family. The $M^{II}N_6$ octahedron is top left and bottom right while the $Pt^{IV}C_6$ octahedron is bottom left and top right (reprinted with permission from [33] © 2006 American Chemical Society).

expand on heating and contract on cooling. You can see this behaviour in the cracking of asphalt on a road for example – the asphalt expands in hot weather and then cracks as it shrinks again in winter. Thermal expansion can be a problem in some materials, causing wear, cracking and stress. However, a composite material that is just the right mixture of a positive thermal expansion material and a compatible negative thermal expansion material would not change size at all with temperature. Such a property would be of tremendous use in high precision optical mirrors, for example. This goal has spurred significant research into negative thermal expansion and the field has redoubled in importance recently with the observation that ZrW_2O_8 contracts over a temperature range in excess of 1000 K.[32] Negative thermal expansion is only of interest to relatively few supramolecular chemists and we will only touch upon it briefly. However it is interesting in the context of framework materials because the principal cause of NTE behaviour is changes in the bending or transverse 'guitar string' type vibrations of a M-L-M unit in a framework material with temperature, Figure 9.33. These structural changes must outweigh the natural tendency of bonds to lengthen with increasing temperature. Typically L in this context is an oxide ligand, but longer multiatomic ligands such as CN^{-} also display this type of behaviour. Examples of coordination polymers exhibiting NTE include $[Ni(CN)_2]_n$ and the Prussian blue analogues $[M^{II}Pt^{IV}(CN)_6]$ (M = Mn, Fe, Co, Ni, Cu, Zn,Cd).[33] Perhaps the most striking material in this context is $Ag_3[Co(CN)_6]$ which exhibits tremendous positive thermal expansion in one direction due to weak $Ag^{+}\cdots Ag^{+}$ interactions that is transmitted by Co-CN-Ag-NC-Co linkages into a 'colossal' NTE along the crystal trigonal axis. Both the positive and negative thermal expansion are an order of magnitude greater than that observed in any other crystalline material.[34]

9.5.6 Interpenetrated Structures

Batten, S. R., 'Topology of interpenetration', *CrystEngComm* 2001, **3**, 67–72.

As we saw for hydrogen bonded diamondoid solids in Section 8.12 interpenetration is defined as the mutual interweaving of two or more independent, unconnected networks such that they cannot be separated without breaking bonds – they are topologically entangled. Thus a single polymer chain passing through a channel in a host net is not interpenetrated – it is simply a guest. We will return to

molecular interpenetration in the next chapter when we talk about the chemistry of catenanes. Two interpenetrated circles would resemble the magic trick involving 'magic rings' that apparently pass through one another to interlink, but, unlike the trick rings, interpenetrated chemical networks are inseparable. When only two networks are interpenetrated we describe the network as twofold interpenetrated. More generally networks can be *n*-fold interpenetrated with values of *n* up to 11 being known! Interpenetration is a beautiful phenomenon and it arises from the driving force towards close packing in solids. In networks with large void spaces such as expanded diamondoid nets (in which there is a very large hole in the middle of the adamantoid unit) the solid is unstable because there is a lack of van der Waals interactions at the surface of the cavity. If the cavity can be removed those interactions are restored. There are two ways in which the space can be filled; either through the inclusion of guests to give a potentially porous solid, or by interpenetration of additional, independent networks. From the point of view of designing porosity, therefore, interpenetration is a considerable hindrance.

The nomenclature for interpenetration takes the form *m*D→*n*D where *m*D is the dimensionality of the individual independent networks (in the present case coordination polymer networks) and *n*D is the dimensionality of the resultant interpenetrating system. The networks are also described as *parallel* or *inclined* depending on whether the interpenetrated polymers propagate in parallel directions or at a significant angle to one another. For networks which involve interpenetration between networks of different dimensions, then *m*D is replaced by *m*D/*p*D. For interpenetrating nets which have the same dimensionality but different topology, *m*D is replaced by *m*D/*m*D. For 2D inclined interpenetration, only a 3D entanglement is possible, so the →3D is redundant and omitted. Similarly, for 3D interpenetration, everything from the arrow onwards in the nomenclature is also not needed.

A survey of 301 interpenetrated structures in the CSD and ICSD was undertaken in 2004 which showed the distribution of structure types given in Figure 9.34. The 3D diamondoid net with its large adamantoid cavities proved to be by far the most common interpenetrated solid. For coordination polymers the highest degree of interpenetration is 10-fold and occurs for a silver(I) complex of 1,12-dodecanedinitrile. This simple ligand in fact forms three different diamondoid nets with Ag(I) of formula [Ag(1,12-dodecanedinitrile)$_2$]X with the Ag^+ ions acting as tetrahedral 4-connected nodes.[35] The degree of interpenetration depends on the anion with fourfold interpenetration in the ClO_4^- salt, eightfold with PF_6^- and AsF_6^-, and tenfold with NO_3^-. The eightfold structures are strictly an interpenetration of two normal fourfold interpenetrated diamondoid networks and have

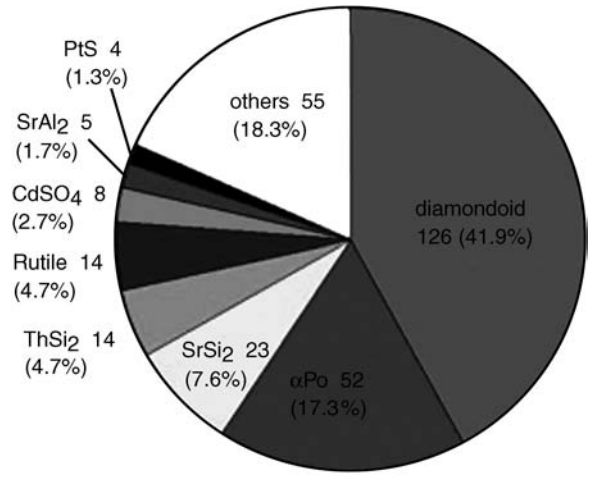

Figure 9.34 Distribution of the topologies within the 301 interpenetrated structures observed in the CSD and ICSD (reproduced with permission of The Royal Society of Chemistry).

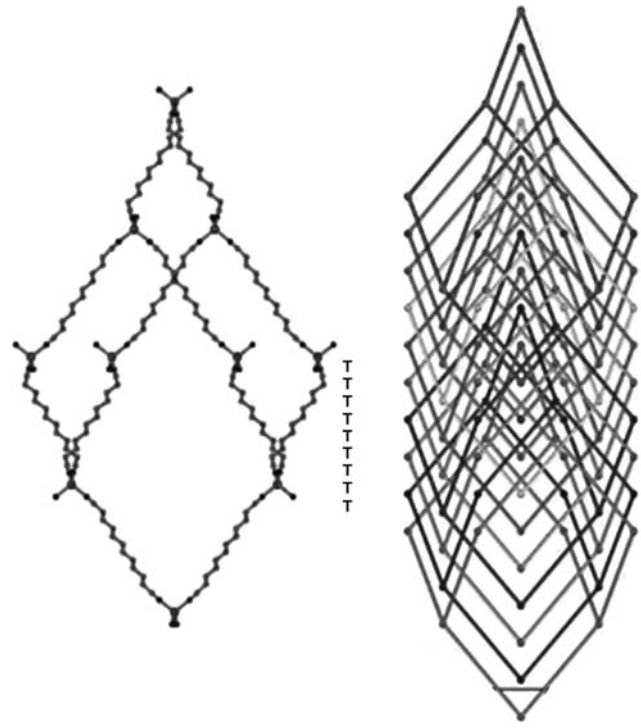

Figure 9.35 The adamantoid cage and schematic of the tenfold interpenetration in [Ag(1,12-dodecanedinitrile)$_2$]NO_3 – all of the torsion angles of the ligand are *trans* (T) maximising its length (Copyright Wiley-VCH Verlag GmbH & Co. KGaA. Reproduced by permission). See plate section for colour version of this image.

been described as [4+4]-fold interpenetrated. The different anions cause changes in the torsion angles in the ligand, changing its length. Thus the nitrate compound has all *trans* torsions and the ligand adopts the conformation with the maximum length. In the [4+4] interpenetrated complex half of the ligand have two *gauche* torsions, one at each end, and in the fourfold structure all of the ligands have two *gauche* angles. The ten independent networks in the nitrate salt are shown in Figure 9.35.

The topologically simplest networks are 1D→1D parallel networks but few are known for coordination polymers. A hydrogen bonded example is the co-crystal of 4,4′-dipyridylpropane (**9.12**) and 4,4′-sulfonyldiphenol (**9.13**), Figure 9.36. One dimensional strands can also give rise to two dimensional

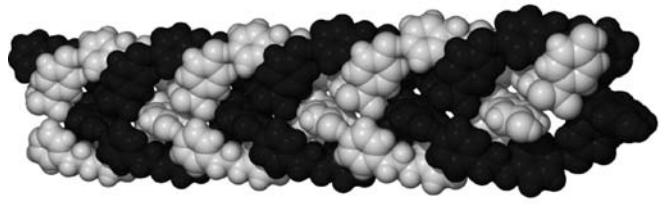

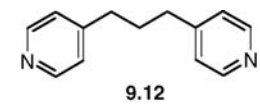

9.12

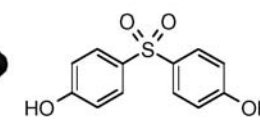

9.13

Figure 9.36 1D→1D parallel interpenetration of hydrogen bonded strands of 4,4'-trimethylenedipyridine **9.12** and 4,4'-sulfonyldiphenol **9.13**.

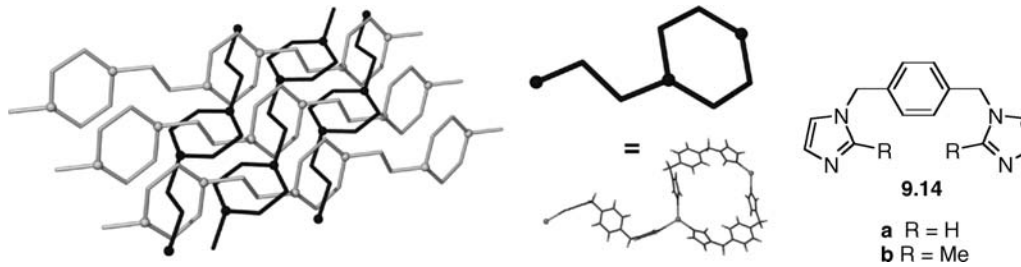

Figure 9.37 1D→2D inclined interpenetration in $[Ag_2(\mathbf{9.14a})_3](NO_3)_2$.[36]

sheets as in the Ag(I) complex of **9.14a** in which 1D strands are threaded through a metallomacrocyclic portion of an independent network to give 1D→2D inclined interpenetration, Figure 9.37.[36] Two dimensional sheets may interpenetrate in three different ways; either 2D→2D parallel, 2D→3D parallel and 2D→3D inclined. The first possibility can only occur if the mean planes of the topologically connected sheets are not offset in the direction perpendicular to the direction of their propagation. One particular nice example is a 'Borromean' 2D→2D parallel net of (6,3) topology with silver ions linked by ligand **9.14b** (Figure 9.38) and lined up by closed shell argentophilic interactions (Section 1.8.9).[37] We will return to the elegant Borromean motif, in which three mutually rings are topologically held together even though no two are interlinked, in the next chapter. Finally, a remarkable comprehensive, annotated and classified list of essentially all known interpenetrated structures is maintained by Stuart Batten at Monash University, Australia (http://www.chem.monash.edu.au/staff/sbatten/interpen/index.html).

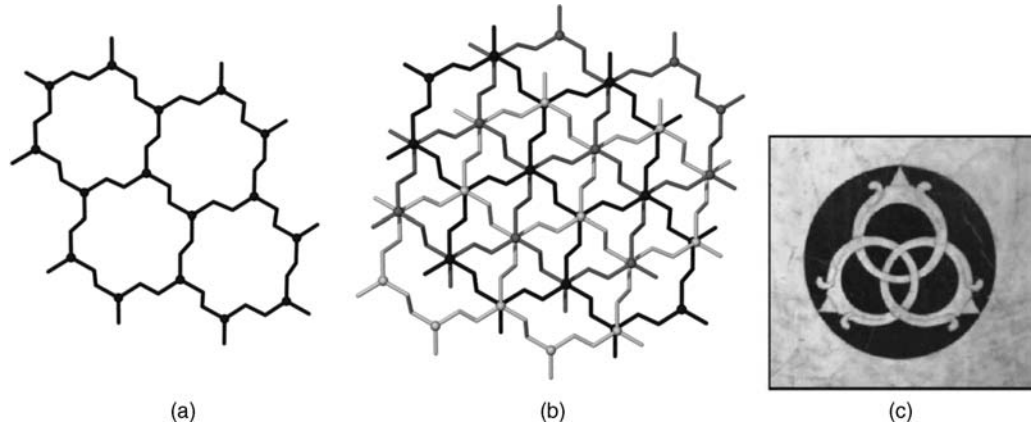

Figure 9.38 (a) A 6,3-sheet of $[Ag_2(\mathbf{9.14b})_3](BF_4)_2$ and (b) the 2D→2D parallel Borromean interpenetrating network that it forms with the means planes of the 2D sheets coincidental. The Ag atoms (spheres) lie above each other, held by argentophilic interactions. (c) Borromean rings in black on white marble at the Cappella Rucellai in the Church of San Pancrazio, now the Marino Marini Museum, in Florence. The rings form part of the coat of arms of the Borromeo family and are also said to be a symbol of the Florentine de Medici family (photograph courtesy of Prof. L. J. Barbour).[37]

9.5.7 Porous and Cavity-Containing Structures

Yaghi, O. M., Li, H. L., Davis, C., Richardson, D. and Groy, T. L., 'Synthetic strategies, structure patterns, and emerging properties in the chemistry of modular porous solids', *Acc. Chem. Res.* 1998, **31**, 474–484.

As we have seen much of the interest in coordination polymers comes from their potential and actual porosity and hence zeolite-like properties – they are often described as 'organic zeolites'. In this chapter we have already encountered a number of compounds with channels and cavities but we have not so far addressed the issue of whether these are porous materials according to the strict definitions given in Section 9.1.3. In coordination polymer chemistry the rational design of microporous and channelled polymeric molecular or supramolecular materials is a challenging, but increasingly fruitful, area of research. Such materials may have key applications in the petrochemicals industry (*cf.* production of simple feedstocks such as methanol by zeolites), separation science and the environment, *e.g.* the destruction of volatile organic compounds (VOCs). The potential for directed chemical reactions within a solid matrix has already been demonstrated for urea inclusion compounds, while the attractive goal of enantiospecific syntheses within chiral frameworks has yet to be realised. To date, much use has been made of microporous silicas and aluminosilicates, such as zeolites, in these kinds of applications because of their thermal robustness (even in the absence of guest) and the malleability of the framework size by use of a templated synthetic approach. Because of the simple nature of the building blocks (tetrahedral fragments such as SiO_4^{4-}) the design of more versatile hosts, including chiral hosts, is not feasible by this method, however. Design of rigid ligands with divergent, carefully placed binding sites offers enormous potential for the synthesis of tailor-made porous materials. In principle, the construction of porous coordination polymers is as simple as choosing a combination of a ligand with more than one binding site that cannot chelate (divergent binding sites), and a metal centre that has complementary divergent coordination sites. The result should be a coordination polymer (*cf.* Figure 9.25). If the ligand is large enough, cavities will be left between one metal node and the next. The situation is not as simple as it seems, however. Metal–ligand interactions are often strong and hence non-labile. As a result, products may deposit rapidly as amorphous powders, and kinetic products of irregular structure are common. This kind of problem may be overcome partially through the use of diffusion, solvothermal (heating in water under pressure) and gel permeation synthetic and crystal growth techniques. Furthermore, the geometry of the metal–ligand interactions is not always easy to predict, and even if a pore structure is generated there is no guarantee that the pores will be accessible to guest molecules from outside the crystal *via* access channels. However, this is a necessary criterion for the use of such designer materials in ion exchange or inclusion reaction type applications. Moreover, as we saw in the last section, carefully designed pores may end up being filled by interpenetration instead of guest-containing channels or cavities. Despite these drawbacks, a great deal of progress has been made in the engineering of porous solids. A broad range of ligands such as 4,4′-bipyridyl (bpy) and expanded analogues such as **9.10–9.12**, carboxylates and other oxygen donors, nitriles, as well as more exotic bridges such as the tetrahedral $Ge_4S_{10}^{4-}$ (**9.15**), have been used as prototype divergent building block ligands.

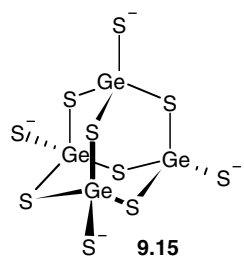

9.15

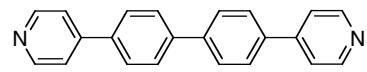

9.16

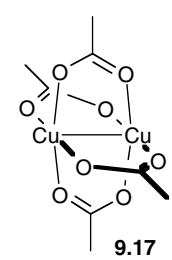

9.17

Bpy in particular forms an enormous variety of porous networks with the network geometry depending on the coordination requirements of the metal centre. Simple networks do not exhibit any interpenetration however, as the complexity increases, two-, three-, four- and six-fold interpenetrated structures are formed, although many still contain pores and channels that include the counter anions (Figure 9.39). The four-fold interpenetrated diamondoid $[Cu(bpy)_2](PF_6)$ contains PF_6^- anions in interstitial sites of 6 Å width, which cannot be exchanged for other anions. In contrast, the more open (although still highly interpenetrated) $[Cu(bpy)_{1.5}](NO_3)\cdot 1.25H_2O$ exhibits anion exchange behaviour once the water is removed by heating. The small NO_3^- can be exchanged for SO_4^{2-} and BF_4^-.[38] Similarly in the extended structure $\{[Ag(\mathbf{9.10})]ClO_4\}_n$ the perchlorate anions can be exchanged for PF_6^- by soaking in $NaPF_6$ solution, but not the other way around. The hexafluorophosphate structure is postulated to be more stable because of increased Ag···Ag interactions.[39] There is considerable debate about the mechanism of these anion exchange processes which could be either involve anions diffusing into and out of a solid microporous host or it could involve a solution-mediated dissolution and recrystallisation process. Strong evidence for the latter has been obtained for the anion exchange coordination polymers $\{[Ag(bpy)]BF_4\}_n$ and $\{[Ag(bpy)]NO_3\}_n$ using a combination of IR and ^{1}H NMR spectroscopy, transmission electron (TEM) and atomic force (AFM) microscopies, and X-ray powder diffraction (PXRD) [40, 41] Hence reports of anion (as opposed to neutral guest) exchange *via* a solid-state mechanism in coordination polymers should be regarded with caution.

Both bpy and the extended bipyridyl ligand (**9.10**) have been used to produce square grid compounds, analogous to Hoffman-type inclusion compounds. The additional two carbon spacer in **9.10** apparently has the effect only of extending the grid dimensions in most cases with the exception of the NbO network

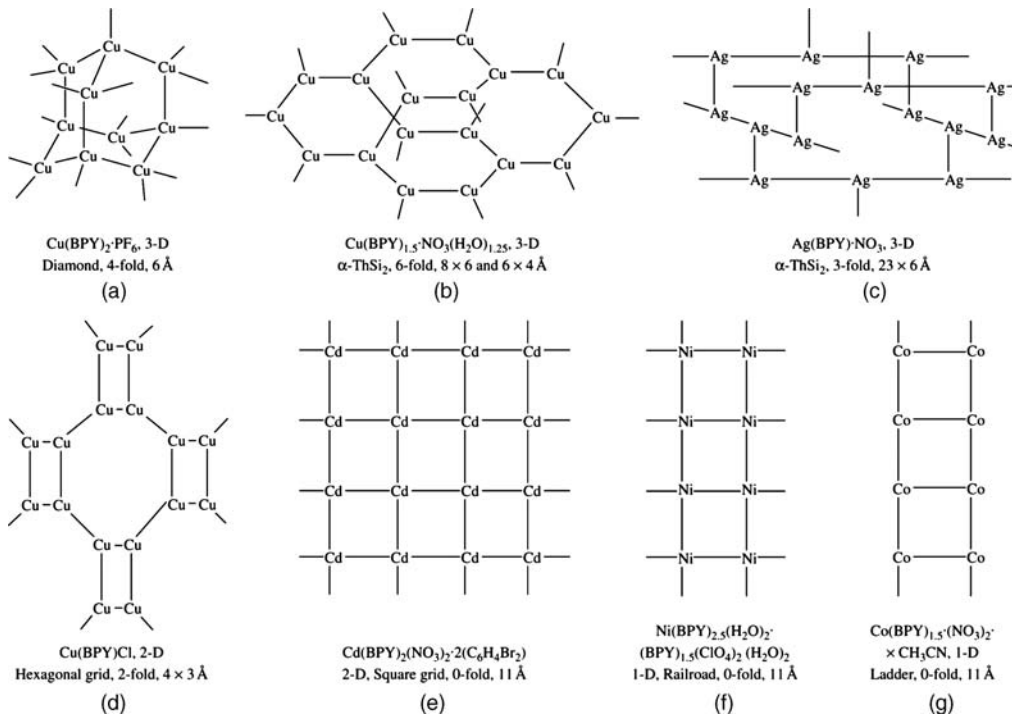

Figure 9.39 Schematic representations of metal 4,4′-bipyridyl porous networks. Lines represent the bipyridyl ligand except for vertical lines in (c), which represent Ag···Ag bonds (2.977 Å long), and horizontal lines in (d) which represent Cu···Cu. The chemical formula, framework dimensionality, structure type, degree of interpenetration and pore aperture are listed under each representation. (Reproduced with permission from Reference 38).

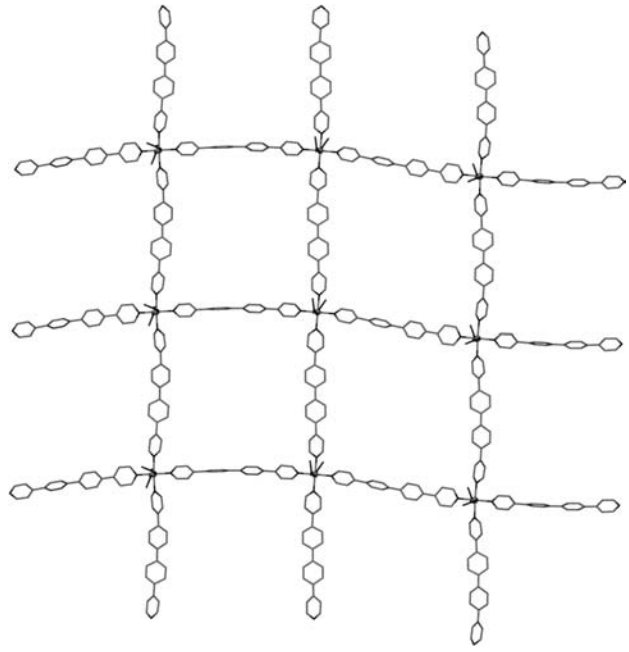

Figure 9.40 2D grid coordination polymer with included o-xylene guests based on the extended bipyridyl **9.16**.[42] (Reprinted with permission from [38] © 1996 American Chemical Society)

noted above. Very long bipyridyl ligands with up to two phenylene spacers (**9.16**) also produce 2D square grid coordination polymers with Ni(II) of formula $\{[Ni(\mathbf{9.16})_2(NO_3)_2]\cdot 4o\text{-xylene}\}_n$ with cavities of dimensions 20 × 20 Å occupied by the xylene guests and channels of cross-section 20 × 10 Å, surprisingly without interpenetration, Figure 9.40.[42] The coordination polymer is truly porous and can withstand guest removal. The framework is stable up to 300 °C because of the relative involatility of the larger ligand.

The dimensionality of bipyridyl-based networks can be reduced by selective blocking of metal coordination sites while the SBU concept can be used to reduce problems of interpenetration. A designer 1D coordination polymer results from the interaction of bipyridylpropane (**9.12**) with the dicopper tetraacetate 'paddlewheel' or 'lantern' SBU $Cu_2(OAc)_4$ (**9.17**) which has two vacant sites, one on each copper(II) ion parallel to the Cu–Cu axis. The result is a parallelogram-shaped grid structure arising from the crossing of 1D strands. A variety of guest molecules such as acetic acid dimers, methanol and ethylene glycol are included into the parallelogram cavities, Figure 9.41. The van der Waals nature of the interactions between the polymer strands, however, means that the host does not survive removal of the guests and so it cannot be regarded as truly porous. Interestingly, however, this material can be prepared by solid state mechanochemical grinding of the metal salt and ligands (Section 8.2.9).[43] Recent work has also shown that even 3D coordination polymers can be synthesised in this way. While mechanochemistry can degrade crystallinity on prolonged grinding, it appears that after a short period of grinding to initiate a reaction, solid-state synthesis of coordination polymer frameworks can continue without further agitation. In general mechanochemistry represents an interesting new approach to coordination polymer synthesis.[44]

While pyridyl-based coordination polymers are extremely synthetically versatile they are not generally particularly thermally robust as a consequence of the tendency of the pyridyl ligands to dissociate or decompose above *ca*. 250–300 °C. The volatility of the ligands is linked to the fact that they are neutral and hence stable in the free state. Moreover their neutrality means that even in the absence of interpenetration, coordination polymer frameworks are generally filled with counter-anions which,

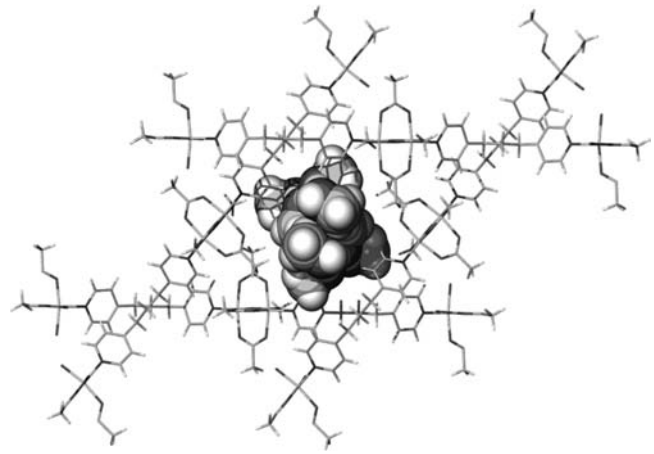

Figure 9.41 Methanol guest inclusion by the 1D coordination polymer $[Cu_2(OAc)_4(\mu\text{-}\mathbf{9.12})]$ (guest shown in space-filling mode.[43])

as we have seen, are difficult to remove without dissolution of the framework. These issues suggest that thermally robust, involatile anionic ligands might make more zeolite-like coordination polymer frameworks. Just such an example comes from the reaction of $[Mn(O_2CCH_3)_2(H_2O)_4]$ with the inorganic ligand **9.15** which gives the elegant diamondoid solid $[NMe_4]_2[MnGe_4S_{10}]$, in which the NMe_4^+ counter ions are included as guests within the large pores in the diamondoid lattice. Heating the material up to 500 °C in an analogous fashion to the preparation of zeolite frameworks (calcination) results in the decomposition of the alkylammonium cation to give the effectively guest-free porous material in which the framework charge is balanced by H^+. The compound is indefinitely stable because of its extremely robust inorganic architecture. The NMe_4^+ cations may be replaced by a variety of divalent metals. In the next section we will see how anionic ligands, in combination with the SBU concept, have finally led to robust, zeolite-like coordination polymers with large pores and highly versatile sorption properties.

9.5.8 Metal-Organic Frameworks

Rowsell, J. L. C., Yaghi, O. M., 'Metal-organic frameworks: a new class of porous materials', *Micropor. Mesopor. Mater.* 2004, **73**, 3–14; James, S. L., 'Metal-organic frameworks', *Chem. Soc. Rev.* 2003, **32**, 276–288.

A key result in the area of porous materials came in 1995 with the synthesis of the first MOF by the group of Omar Yaghi, then at Arizona State University, USA (now Michigan).[45] These researchers prepared **9.18**, a layered coordination polymer based on benzene 1,3,5-tricarboxylic acid (trimesic acid, **9.19**). The spacer units (S) are two pyridine ligands and the whole assembly comprises a two-dimensional sheet coordination polymer. Each sheet interacts with those above and below it by individually weak π–π stacking interactions of the pyridine aromatic rings. Thermogravimetric analysis of the material indicates that it is able to reversibly release aromatic guest molecules from its channel-like pores at 190 °C, yet the overall crystalline host structure is retained up to 350 °C, as demonstrated by X-ray powder diffraction analysis and examination of the crystals by optical microscope. Addition of further guests to the guest-free structure results in their incorporation into the host channels. The overall mode of guest inclusion is reminiscent of Hoffman-type clathrates (Section 9.4) and the thermal robustness and reversibility of the binding suggested that these systems may prove to be of significant practical application.

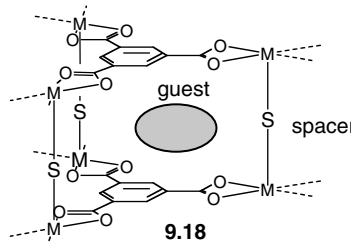

9.18

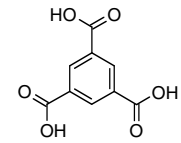

9.19

Four years later in 1999 Yaghi's group reported a 3D MOF termed MOF-5,[46] a compound that has subsequently formed the basis for a huge range of important MOFs and is produced commercially on a large scale. MOF-5 is based on an octahedral zinc(II) oxo-centred SBU (Figure 9.42) that occupies the vertices of a cubic lattice, and bridging terephthalate (1,4-benzene dicarboxylate) dianions, Figure 9.43. The compound is prepared *quasi*-solvothermally and the optimised conditions are very straightforward. An *N*,*N*-diethylformamide solution of $Zn(NO_3)_2{\cdot}4H_2O$ and terephthalic acid is heated at between 85° and 105 °C in a closed vessel to give crystalline MOF-5 in 90 % yield. The use of an octahedral SBU (which is formed under the conditions of synthesis) instead of an octahedral metal centre has the effects of markedly expanding the structure and because of its size it reduces the degree of interpenetration. The structure can be further expanded by the use of larger, linear dicarboxylates ligands to yield *isoreticular structures* (structures with nets of equivalent topology) termed IRMOFs, Figure 9.43. This series of MOFs exhibit square pore windows with diameters up to 19.1 Å while the internal pore diameters are up to 28.6 Å. The size of the MOFs can be controlled by choice of the length of the aromatic region of the dicarboxylate ligands. The calculated densities of the frameworks of materials are as low as 0.21g cm^{-3} which represents the lowest density observed for any crystalline material (compare this number to 1.0 g cm^{-1} for liquid water and about 1.5 g cm^{-3} for normal organic solids). As the spacers become larger the SBU does not entirely prevent interpenetration and in a few cases doubly interpenetrating frameworks have been observed but repeating the syntheses at lower concentration gives analogous non-interpenetrated structures. This dependence on conditions highlights the role that solution speciation has on crystal nucleation. These IRMOF frameworks generally display remarkable stability even at high temperatures (~ 300 °C) and are stable even in the absence of guests and hence are truly porous. Indeed they are remarkably effective at storing gases such as methane after removal of guest solvent. The most effective framework, IRMOF-6, absorbs an amount of methane equivalent to 240 cm^3 per gram of MOF (if the methane were at standard

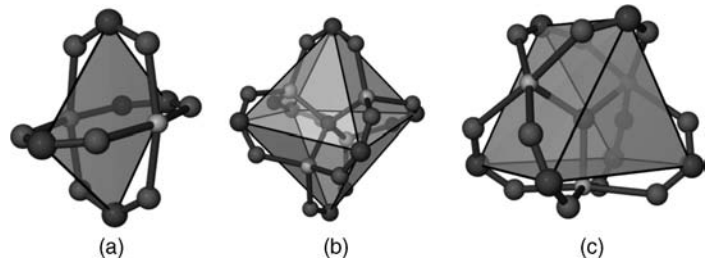

Figure 9.42 Secondary Building Units (SBU) using carboxylates with rigid coordination geometries that replace metal ions as vertices in MOFs. (a) Paddlewheel or lantern structure as in **9.17**, (b) octahedral 'basic zinc acetate' SBU used in MOF-5 and (c) a trigonal prismatic oxo-centred trimer. The polyhedra use carboxylate carbon atoms as their vertices and the MOFs propagate *via* the linkers attached to these carbon atoms. The metal atoms are bound to only terminal ligands in addition to those shown.

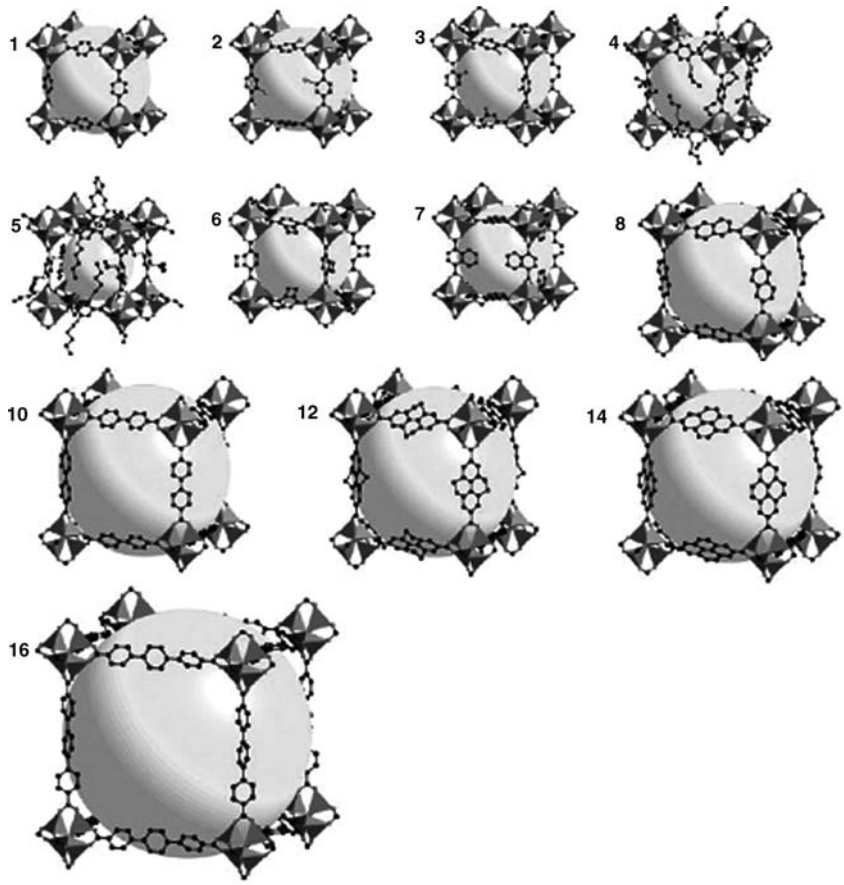

Figure 9.43 Single crystal X-ray structures of IRMOF-*n* ($n = 1 - 7, 8, 10, 12, 14$, and 16), labelled respectively. MOF-5 is re-designated IRMOF-1 as part of this series. IRMOFs 9, 11, 13, and 15 are doubly interpenetrated. Zn(II) tetrahedral shown as polyhedra. The large spheres represent the largest van der Waals spheres that fit in the cavities without touching the frameworks (reprinted from [47] with permission from AAAS).

temperature and pressure). The methane is adsorbed at 298 K and under 36 atm pressure. This represents 70 per cent of the compression achieved in methane cylinders which operate at over 200 atm.

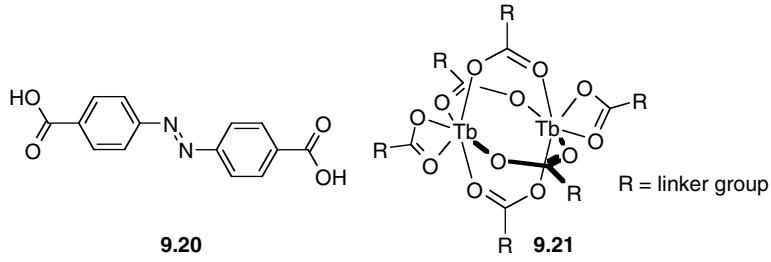

9.20 **9.21**

The way in which SBU size affects interpenetration has been investigated systematically and theoretically for the terbium(III) SBU **9.21** with the extended dicarboxylate **9.20**. These components crystallise from DMSO to give MOF-9, a doubly interpenetrated cubic network with significant void space filled by DMSO molecules. The question arose as to whether the observed doubly interpenetrated network is the maximum degree of interpenetration possible given the size of the SBU. The compound can be described

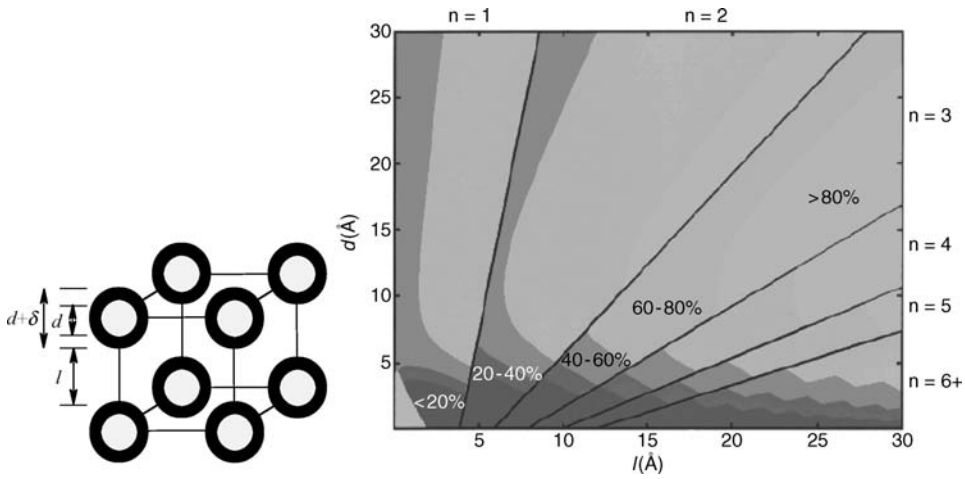

Figure 9.44 Geometrical parameters used in equation 9.1 and free volume/interpenetration plot for compounds related to MOF-9. Interpenetration n is plotted (total number of frameworks in a structure) as a function of d (diameter of an SBU) and l (length of linker) with the corresponding free volume expressed as percent of crystal volume shown in decreasing shades of darkness (darkest: <20 to lightest: >80%). The solid dark lines for n =1 to n = 6 + were obtained according to equation 9.1 (see text) and assuming a C connector with δ = 3.4 Å (van der Waals diameter of a C atom) and linkers with negligibly small diameter. For the volume calculation the SBUs diameter was considered d and the volume of the linker was based on a cylinder of a diameter ($2r$) equivalent to that of a benzene ring (5 Å) and a length l. Thus, the free volume was calculated based on the following: Volume of the cell = $(d + l)^3$; volume occupied by SBUs/cell = $n(\pi/6)d^3$; and volume of the linkers/cell = $3n[(\pi r^2)]l$. (Reprinted with permission from [48] © 2000 American Chemical Society).

by a geometric model based on two interpenetrating cubic frameworks in which the vertices where the SBU are situated are approximated as large spheres. The maximum degree of interpenetration, n, is related to the diameter of the SBU, d, the length of the linker, l, and the van der Waals radius of the atom joining the SBU and linker, $\delta/2$ (Figure 9.44). The unit cell edge length $a = d + l$. For n frameworks to interpenetrate with the centres of their SBUs aligned along a body diagonal, $n(d + \delta) = \sqrt{3}a$; thus,

$$n \leq \sqrt{3}\,\frac{d+l}{d+\delta}$$

This relationship can be used to predict the consequences of d and l for the percentage free volume in cubic structures that interpenetrate to the maximum possible degree given the bulk of the components, Figure 9.44. The conclusion is that the n = 2 structure observed is indeed the most interpenetrated possible, *i.e.* it is *maximally interpenetrated* as a consequence of the size of the SBU.

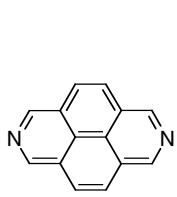

9.22

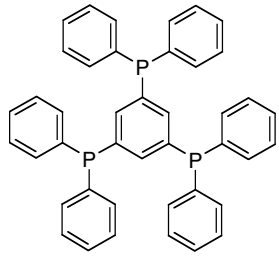

9.23

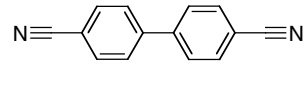

9.24

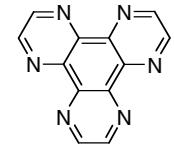

9.25

Interpenetration has also been reduced by the use of large bridging ligands, such as **9.22** in place of bpy, which reduces interpenetration from fourfold to threefold in the case of the diamondoid [Cu(**9.22**)](PF_6),[49] and in the case of the very bulky **9.23** where the framework [Ag_4(**9.23**)$_3$(CF_3SO_3)$_4$] exists as a non-interpenetrated hexagonal structure with large 72 membered rings of width 16–18.4 Å.[50] Conversely, nitrile ligands such as **9.24** tend to increase interpenetration because they do not have much steric bulk at the metal centre, *e.g.* the ninefold interpenetrated structure of [Ag(**9.24**)$_2$](PF_6).

The remarkable porosity of zeolite-type compounds stems from the intrinsically robust nature of the Al-O-Si and Si-O-Si linkers and their relative chemical inertness (they don't react with oxygen when heated to very high temperatures, for example). Generally MOFs do not exhibit such thermal stability and linkers can be labile, and hence loss of crystallinity of guest removal or on heating. However, there are now a number of MOFs that undergo very little framework change upon adsorption or desorption of guests. Such frameworks can even be based on pyridyl type ligands, as in [Ni_2(bpy)$_3$(NO_3)$_4$] which exhibits little structural change on removal of adsorbed ethanol from its 6 × 3 Å channels at 100 °C. If the empty framework is exposed to ethanol the original structure is regained. Interesting 'step' type adsorption behaviour that deviates from the type I isotherm (Section 7.11) observed for ethanol is observed for methanol vapour, however, in which initial adsorption is fast, corresponding to hydrogen bonding of the methanol guest to the nitrate anions, followed by a slower structural rearrangement of the adsorbed guests that allows additional methanol incorporation.[51] Another interesting material is the pyrazene (**9.27**) based MOF [Cu_2(**9.26**)$_2$(pyrazene)] which exhibits permanent one-dimensional channels of cross-section 4 × 6 Å. This compound has hydrogen bond basic oxygen atom sites that interact with guest water in the assynthesised material. The water can be removed without altering the framework and the empty host proves to selectively adsorb hydrogen bond acidic guests such as acetylene in preference to non hydrogen bond acids such as CO_2. Acetylene is a very useful chemical feedstock but is often contaminated with other gases such as CO_2. It is a highly reactive molecule which cannot be compressed above 20 atmospheres or it explodes even without oxygen, at room temperature. Hence safe materials for C_2H_2 separation and storage are of significant interest. The acetylene sorption capacity in [Cu_2(**9.26**)$_2$(pyrazene)] is 42 cm^3 (at stp) per gram of host material corresponding to one acetylene per framework formula unit. In comparison only 26 cm^3 g^{-1} CO_2 is adsorbed.[52] Hydrogen bonding to the host non-coordinated oxygen atoms means that the acetylene molecules are held at a periodic distance from one another within the channels. This results in a 'confinement effect' which permits the stable storage of acetylene at a density 200 times the safe compression limit of the free gas at room temperature.

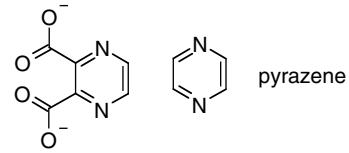

9.26 **9.27**

As a general principle framework robustness is improved by the use of chelate ligands and a good match between metal and ligand hard/soft acid/base properties (Section 3.1) leading to high bond strength, as in lanthanide carboxylates, which often form some of the most stable MOF type materials. Chelating pyridyl type ligands such as **9.25** have been used in MOFs, as in [Ag(**9.25**)(ClO_4)] · 2NO_2Me. This material undergoes reversible exchange of the nitromethane guests for atmospheric water without loss of framework integrity. It is this chelation or bridging within an SBU by multidentate carboxylates,

in combination with the use of rigid aromatic rings as spacers and their 3D connectivity, that makes the IRMOFs and compounds like them particularly robust and useful in porosity-dependent applications such as gas storage. In the final section in this chapter we will look at the particular interest surrounding the use of MOFs in catalysis and hydrogen storage.

9.5.9 Catalysis by MOFs

Horike, S., Dincă, M., Tamaki, K. and Long, J. R., 'Size-selective lewis acid catalysis in a microporous metal-organic framework with exposed Mn^{2+} coordination sites', *J. Am. Chem. Soc.* 2008, **130**, 5854–5855.

It is a particularly attractive research goal to use MOFs as solid state catalysts in an analogous way to zeolites, with all the concomitant advantages of heterogeneous catalysis such as easy product and catalyst separation and with the added advantage of the tunability offered by MOFs, including framework chirality. However intra-cavity catalysis of many chemical reactions by MOFs is not trivial to achieve because it requires the incorporation of catalytically active sites in the MOF. The active site must be able to carry out the desired chemistry yet not react with the MOF ligands nor lose its activity upon prolonged exposure to other potential guest species. This is a significant challenge given the relatively reactive nature of MOFs compared to zeolite frameworks and the traditional kinds of MOFs that have coordinatively saturated metal centres accompanied by robust chelating ligands. Significant progress is beginning to be made in MOF catalysis, however, including enantioselective catalysis, and we highlight just one very interesting recent example here. The MOF $Mn_3[(Mn_4Cl)_3(BTT)_8(CH_3OH)_{10}]_2$ (H_3BTT = 1,3,5-benzenetristetrazol-5-yl) is known to act as an effective H_2 sorbent because of its large pores. The material also has Mn^{2+} ions exposed on the surface of the framework which might act as Lewis acid catalytic sites. The compound has been found to catalyze the cyanosilylation of aromatic aldehydes and ketones. It also carries out the Mukaiyama-aldol reaction – a reaction this is not quite so facile. Because the reaction occurs within the confines of the MOF framework cavities there is a significant degree of size-selectivity in the products obtained which is in line with the known cavity dimensions of the material. This aldehydes bearing smaller substituents such as phenyl and napthyl reacy readily because the product can fit within the zeolite, while aldehydes bearing larger substituents react only sluggishly, Figure 9.45.

9.5.10 Hydrogen Storage by MOFs

Rowsell, J. L. C. and Yaghi, O. M., 'Strategies for hydrogen storage in metal-organic frameworks', *Angew. Chem., Int. Ed.* 2005, **44**, 4670–4679.

We have already discussed the technological importance of hydrogen storage materials in Section 7.9, where we looked at clathrate-type organic frameworks in this context. We now return to the subject

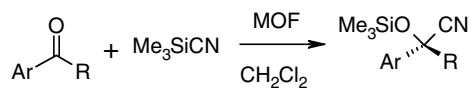

Figure 9.45 MOF catalysed cyanosilylation reaction – when Ar is phenyl or napthyl the product can pass freely through the pores giving yields of over 90 per cent. When Ar = 4-phenoxyphenyl or biphenyl the yields are below 20 per cent because the molecules do not fit readily within the cavities.

with a case study on recent progress in hydrogen storage within MOFs. Hydrogen storage by intrinsically low density materials is of key importance as part of the emerging hydrogen economy. They are particularly crucial in 'green' hydrogen fuel cell based transport applications where there is a vital need to store sufficient hydrogen to power a vehicle over a reasonable journey length (taken to be *ca*. 300 miles or 480 km) without making the energy cost in transporting the storage apparatus (the hydrogen 'fuel tank') prohibitive.[53] The holy grail in this area is a material that meets the US DOE 2010 and, ultimately, 2015 energy density targets (including container and recharge/discharge apparatus). For 2010 these are 7.2 MJ kg^{-1} and 5.4 MJ L^{-1}, which translates as 6.0 weight percent and a volumetric density of 45 kg hydrogen per cubic metre. The 2015 targets, the sort of levels that would be of serious interest to automobile manufacturers, are 9.0 weight percent and 81 kg hydrogen per m^3. For comparison mass density of elemental hydrogen is only 70.8 kg m^{-3} as a liquid at 20 K (1 atm) and 5 kg of hydrogen gas occupies 56 m^3 under ambient conditions (ignoring container mass of course). Given the higher energy density of hydrogen as a fuel and the greater efficiency of fuel cells compared to conventional combustion engines only about 4–10 kg of hydrogen is actually needed and demonstration 'concept cars' have achieved the 2010 specifications using cylinders of hydrogen either under pressure or at cryogenic temperatures. The 2015 targets, however, are not within easy reach by these methods.

So, how do MOFs currently stack up in the hydrogen storage stakes, and what is their future potential? Current MOF research indicates that micro or mesoporous MOFs with significant interactions between the hydrogen and the channel walls are likely to be the most promising materials – adsorption of a second and subsequent layers of hydrogen is really quite weak and so homogeneous, very large diameter pores are not likely to be as useful and hence a large pore surface area is an important property. Moreover hydrogen storage with the H–H bond intact is likely to make for the best discharge and recharge efficiencies and speed. However, given the mass of the framework, and the low mass of the H_2 molecule storage of many moles of hydrogen per mole of framework is necessary and of course the best frameworks will make use of light atoms, particularly light metals, not heavy transition metals or lanthanides.

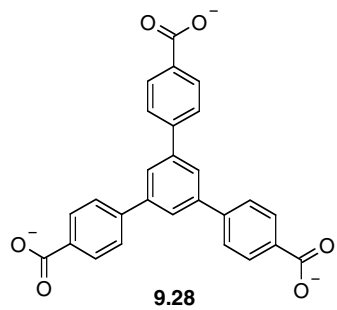

9.28

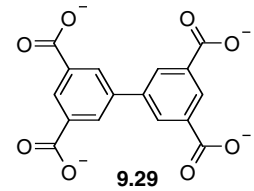

9.29

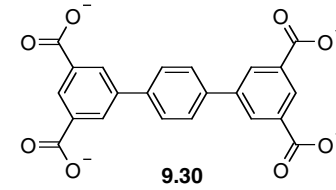

9.30

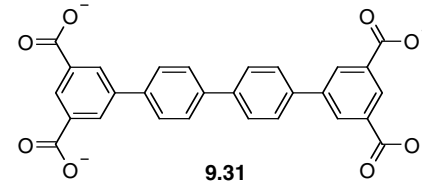

9.31

In terms of surface area MOFs have very promising properties. The largest currently known surface area for a microporous material is MOF-177, a material that uses the octahedral 'basic zinc acetate' SBU (Figure 9.42b) in conjunction with the tricarboxylate **9.28**. At 77 K this compound exhibits an N_2 adsorption-based monolayer-equivalent surface area of 4500 $m^2\ g^{-1}$ and a micropore volume of 0.69 $cm^3\ cm^{-3}$. The compound does not absorb as much hydrogen at lower pressures as other materials with smaller surface areas, however, possibly because of its structure comprising large cavities *ca*. 11 Å in diameter linked by narrower channels. This result highlights the need for a better understanding and careful engineering of surface structure and pore/channel shape as well as just surface area. At high pressure MOF-177 is extremely impressive, adsorbing 7.3 weight percent at 50 bar, Figure 9.46. The

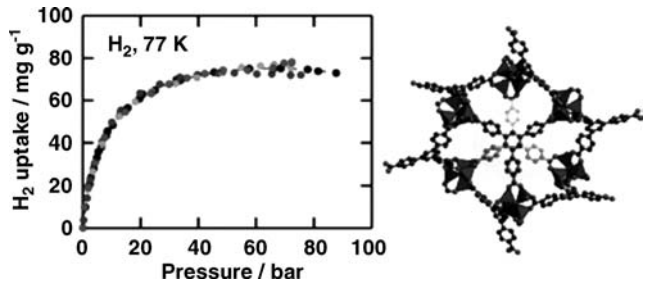

Figure 9.46 Hydrogen adsorption isotherm at 77 K and X-ray crystal structure of MOF-177 (reproduced with permission of The Royal Society of Chemistry).

adsorption is best described by a micropore filling model and so the hydrogen fills much of the cavity (the estimated total capacity is *ca.* 11 weight per cent) as well as being surface adsorbed in the pores.[54] Among the IRMOF series, the best results are obtained for IRMOF-8 which stores up to 2.0 per cent by weight of hydrogen at 298 K and 10 atmospheres pressure. Hydrogen storage at ambient temperature is an ideal situation, however capacity increases as temperature goes down because of the longer residence time of adsorbed hydrogen on the micropore walls and hence for reasons of ease of measurement results are often reported at 77 K and one atmosphere pressure.

Optimal packing of hydrogen would be in a pore that equates to its diameter giving equivalent interactions all around. The kinetic diameter of hydrogen is larger than some gases at 2.89 Å, but this value is clearly much smaller than some of the pore sizes we have encountered and hence there is a possibility of 'wasted space' at monolayer coverage. Hence a highly segmented material with smaller pores is desirable. However, the thickness of the walls of the segment reduces the efficiency and hence a compromise must be reached. In a series of MOFs based on **9.29**–**9.31** of formula $[Cu_2(L)(H_2O)_2]$ (L = **9.29**–**9.31**) all based on the dicopper tetracarboxylate 'paddlewheel' SBU (Figure 9.42a) and with NbO topology, the Nottingham group led by Martin Schröder and Neil Champness showed that the largest pore material is not necessarily the best at hydrogen uptake. In these materials the pores are all of similar shape, occupying 63.3, 70.4 and 75.5 per cent of the crystals, respectively. The pore volumes calculated from the maximum amount of N_2 adsorbed are 0.680, 0.886 and 1.138 cm^3 g^{-1}, respectively for the three materials. Hence there is a relationship between the ligand length and pore size. Hydrogen uptake results showed, however, that it is the intermediate pore size material based on **9.30** that exhibits the most hydrogen uptake, reaching a maximum value of 43.6 g L^{-1}, close to the 45 g L^{-1} specified by the 2010 DOE target. Gravimetrically this corresponds to 2.52 weight percent at one atmosphere pressure and an impressive 6.06 weight percent at 20 atmospheres and 78 K, or 7.8 % at 60 atmospheres.[55] The efficacy of the intermediate material is attributed to a good balance between pore volume and surface area.

Another strategy for increasing hydrogen absorption by MOFs is to include metal atoms with vacant coordination sites that can specifically form σ-bonded H_2 complexes. Many SBU have coordination sites that are only occupied by weakly coordinating ligands that can be displaced by heating. This opens the possibility of chemisorption of H_2. A related development is the phenomenon of catalytic 'spillover'. Spillover involves the splitting of H_2 into hydrogen atoms by small particles of a finely divided metal catalyst such as platinum. If the catalyst is in good contact with the storage material then the hydrogen atoms are included in a way that is poorly understood but results in tangible benefits to their storage ability. For example, hydrogen uptake by MOF-5 and IRMOF-8 can be enhanced by a factor of 3.3 and 3.1, respectively (to nearly 2 wt % at 10 MPa and 298 K). The binding isotherms are fully reversible implying that the spillover hydrogen atoms are also readily recombined into H_2.[56]

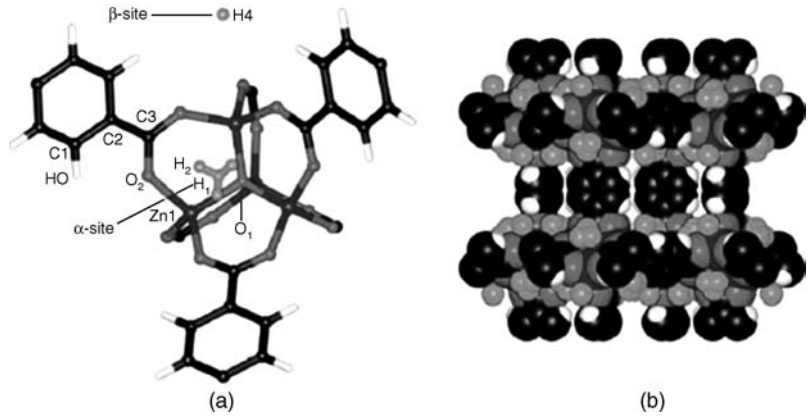

Figure 9.47 (a) The location of the hydrogen absorption sites at 5 K relative to the framework atoms. The α-site is 100% occupied at 50 K, 30 K and 5 K The H_2 molecule is disordered over three possible orientations of which the atoms labelled H1 and H2 represent one possibility. The β-site is 98% occupied at 5 K. (b) Space-filling diagram of one of the framework cavities at 5 K showing the hydrogen positions (reproduced with permission of The Royal Society of Chemistry).

MOF hydrogen sorption chemistry has been dogged by a series of claims of high storage capacity followed by retractions or corrections and the variations in pressures, temperature and conditions make it difficult to compare results. Hydrogen sorption is extremely difficult to measure precisely and the slightest leaks or impurities in the gas significantly distort results because most contaminant gases are adsorbed more strongly than hydrogen. Indeed it is generally accepted as good practice to check H_2 sorption data by performing the analogous experiments with D_2. In addition to the systems already described, among the most impressive MOFs is one reported by the group of Férey (Versailles, France) who have produced the cubic zeotype MOF $[Cr_3F(H_2O)_2(\text{terephthalate})_3]\cdot nH_2O$ (n = *ca.* 25). The compound has a very large cell volume of *ca.* 702 000 $Å^3$ and exhibits a hierarchy of large pores. The nitrogen sorption derived pore volume is 2.0 $cm^3\ g^{-1}$ giving a surface area of *ca.* 5900 $m^2\ g^{-1}$. This interesting material adsorbs 4.5 weight per cent hydrogen at 77 K and 30 atmospheres, although it is not yet certain that this is a maximum value.[57]

The precise site(s) of hydrogen adsorption in MOF-5 has been probed by single crystal neutron diffraction by the group of Judith Howard (Durham, UK).[58] Neutrons are much better than X-ray at precisely locating hydrogen – Box 8.1. The results for data recorded at several temperature from 5 to 120 K are shown in Figure 9.47. Hydrogen sorption occurs at quite specific sites at low loading (1 atmosphere pressure) with the α-site near the SBU node being the most favoured.

Summary

- Robust inorganic porous networks such as zeolites are of tremendous industrial interest in separation, storage and catalysis. As a result they have stimulated the preparation of a wider range of 'organic zeolites' that aim to mimic their porous and robust properties while allowing more extensive synthetic tenability.
- The term 'porosity' requires a demonstration of permeability and is applied to a particular solid form, not just to a particular chemical substance.